Paleoproterozoic Gneissic Granites in the Liaoji Mobile Belt, North China Craton: Implications for Tectonic Setting

7

Mingchun Yang, Bin Chen, and Cong Yan

Abstract

Voluminous Paleoproterozoic gneissic granites occur in the Liaoji belt in the North China Craton (NCC), which were intruded by mafic dykes, and experienced a late-stage amphibolite facies metamorphism. These granites were thought by some researchers to be A-type granites and formed in a continental rifting setting. We propose a different model for the origin of these granites and the tectonic setting, based on the integrated field, petrographic, geochronological, and geochemical studies on a couple of gneissic granite plutons. The gneissic granites were emplaced at 2173–2203 Ma, and the mafic dykes at ca. 2159 Ma, followed by an amphibolite facies metamorphism at ca. 1.9 Ga. The gneissic granites contain mafic microgranular enclaves (MMEs), calcium hornblendes, magnesio-horblendes, accessory titanite, and pyrrhotite. They show calc-alkaline arc magma affinity, with A/CNK = 0.9 − 1.2 (mostly less than 1.1), A/NK = 0.9 − 1.4, SiO_2 = 68.3 − 76.9 wt %, low contents of TiO_2 (<0.3 wt%), enrichment of LILEs, such as K, Rb, Sr, Cs, depletion of some HFSEs, such as Nb, Ti. These characteristics suggest that these gneissic granites are I-type granites formed probably in a subduction zone. The A-type-like characteristics for some granites (the Dafangshen granite) are attributable to the highly evolved nature of the pluton as shown by the high SiO_2 contents (76.7–77.1 wt%), which could have been caused by the high boron contents of the pluton, because addition of boron in magma system tends to prolong magma evolution and lead to significant differentiation. The large variation of whole-rock $\varepsilon_{Nd}(t)$ values (−8.6 to 1.5) and zircon $\varepsilon_{Hf}(t)$ values (−1.3 to 5.6), together with the existence and petrographic features of the MMEs, and oscillatory zoning in plagioclase, suggest that mixing/mingling of lower crust-derived felsic magma with enriched mantle-derived mafic magma might have resulted in formation of these gneissic granites. The existence of Archean inherited zircons in these granites together with the arc affinity suggests a northward subduction for the JLJB in the Paleoproterozoic times.

Keywords

Gneissic granites • Subduction • Arc magmatism • Paleoproterozoic • North China Craton

M. Yang
China Ocean Press, State Oceanic Administration, Beijing, 100081, People's Republic of China

B. Chen (✉)
School of Resources and Environmental Engineering, Hefei University of Technology, Hefei, 230009, Anhui, China
e-mail: binchen@pku.edu.cn

C. Yan
Sinochem Petroleum Exploration & Production Co., LTD, Sinochem Group, Beijing, 100031, People's Republic of China

7.1 Geological Setting of the Liaoji Belt

The Liaoji orogenic belt is one of the three Paleoproterozoic mobile belts on the NCC, located in the eastern part of the Eastern Block (Fig. 7.1; Luo et al. 2008; Zhao et al. 2005). The belt consists of greenschist to lower amphibolite facies metasedimentary, metavolcanic successions, meta-granitic

M. Zhai et al. (eds.), *Main Tectonic Events and Metallogeny of the North China Craton*, Springer Geology, DOI 10.1007/978-981-10-1064-4_7

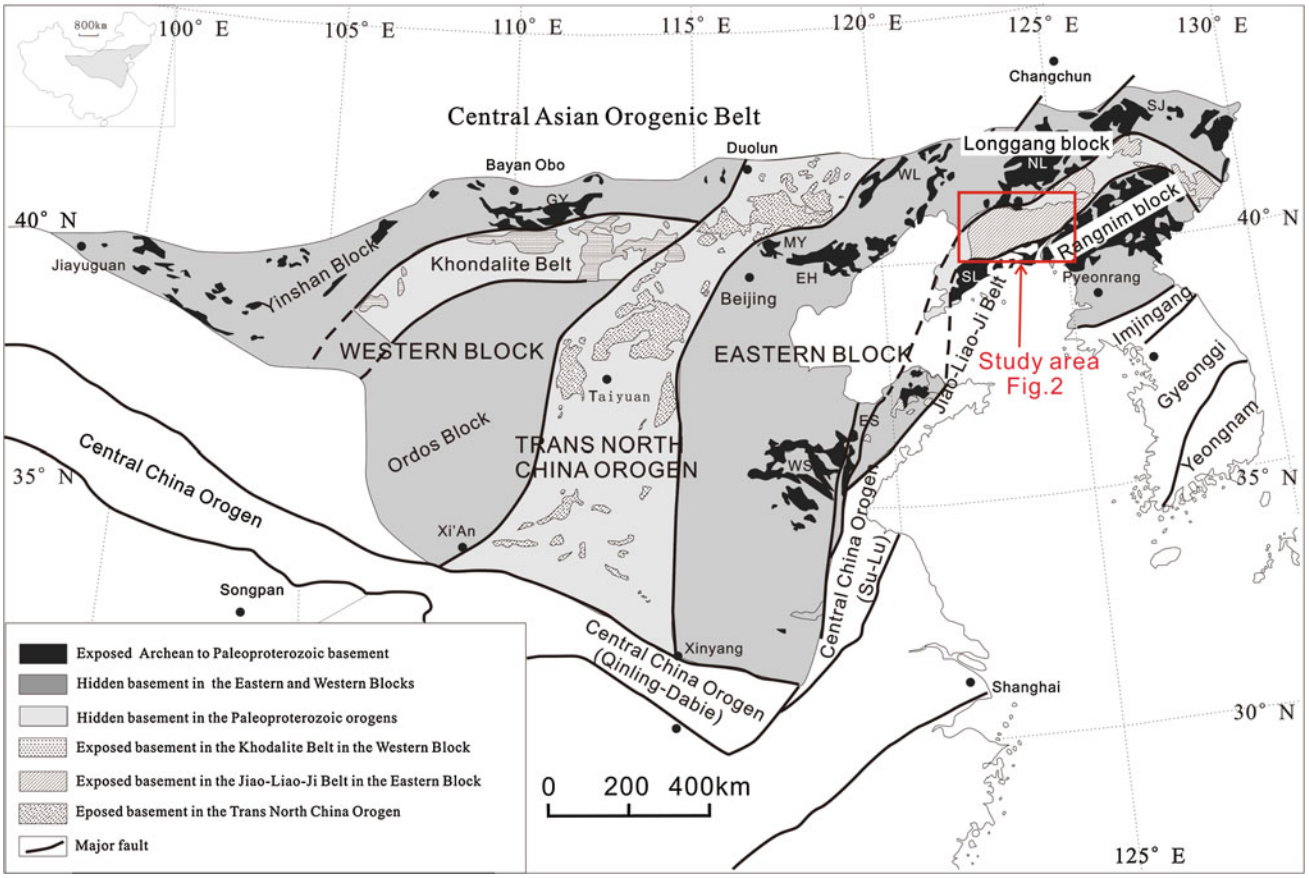

Fig. 7.1 The tectonic subdivision of the North China Craton (after Zhao et al. 2005); also shown is the Jiao-Liao-Ji Paleoproterozoic belt

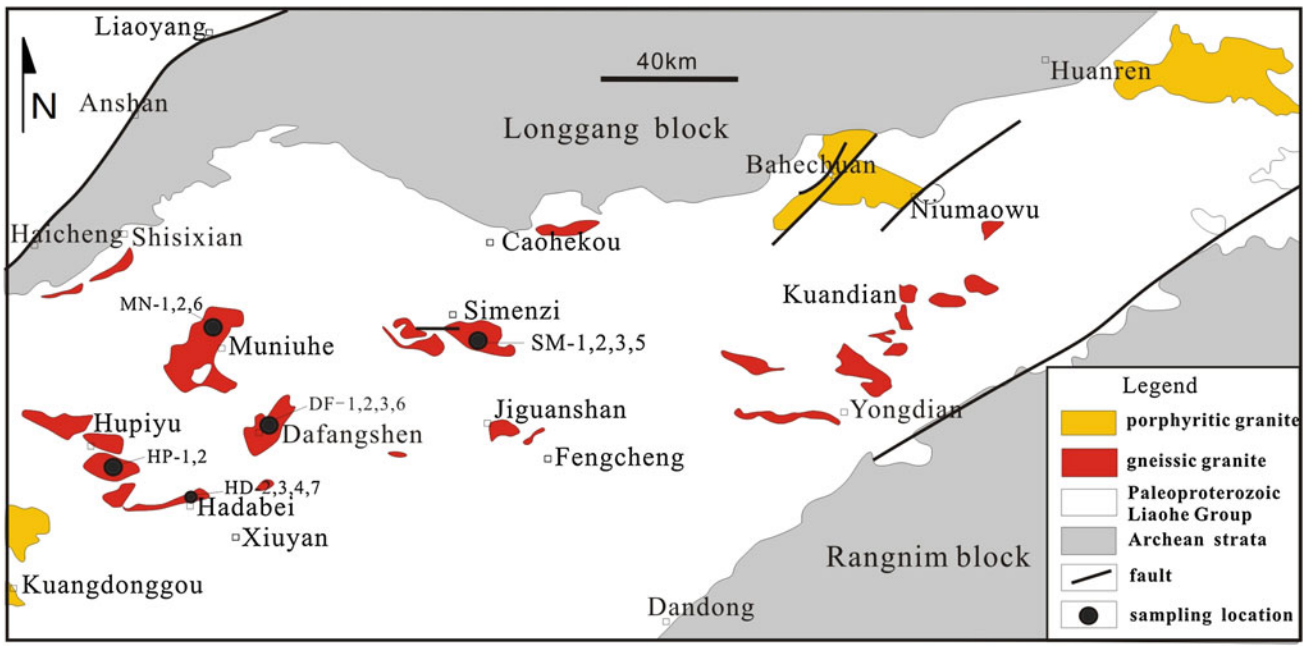

Fig. 7.2 Sketch geological map of the Paleoproterozoic granites in the Jiao-Liao-Ji Belt (after Hao et al. 2004), with sampling localities

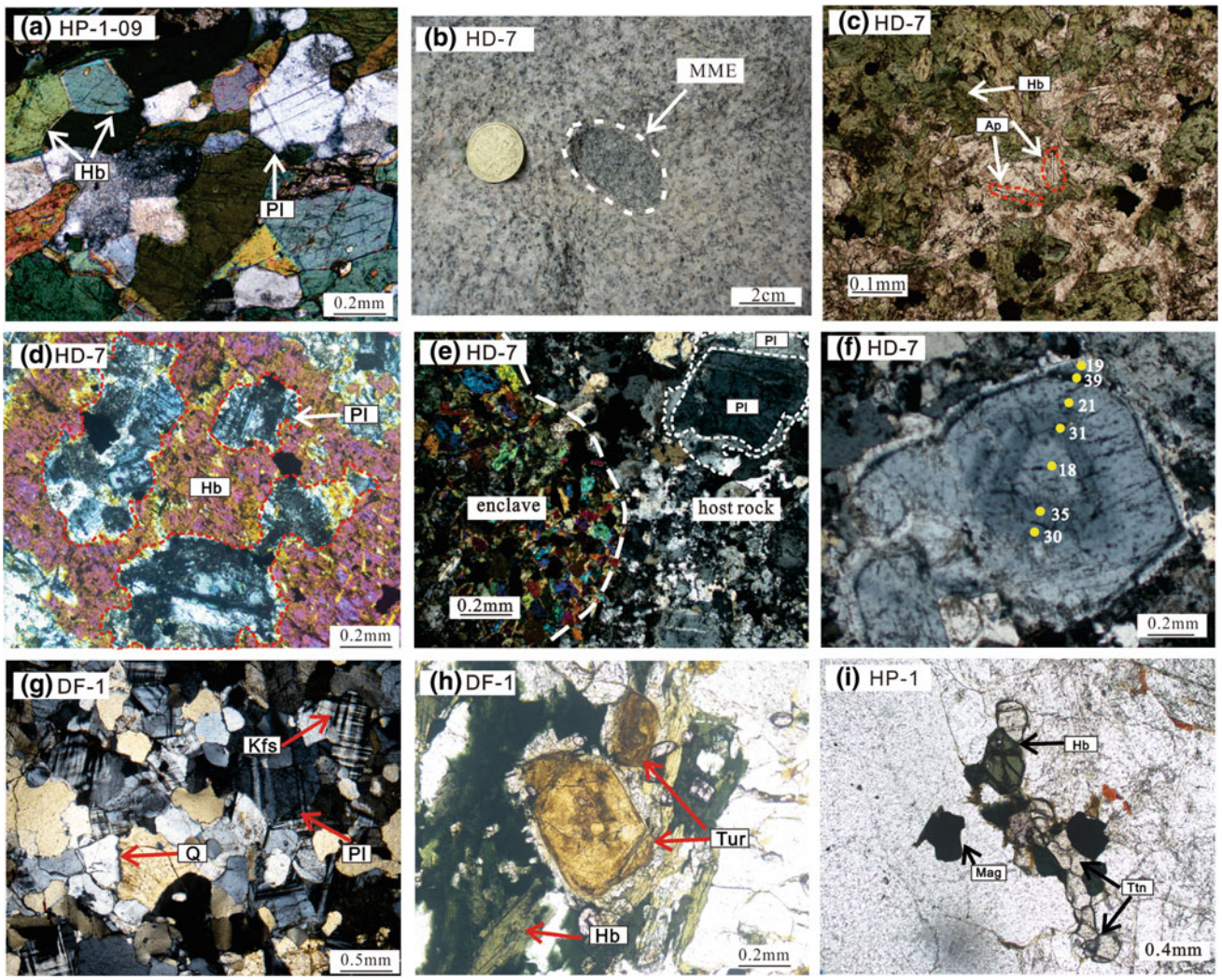

Fig. 7.3 **a** Microphotograph of amphibolite intruded into the Hupiyu gneissic granite pluton; **b** field photo of a mafic enclave from the Hadabei pluton; **c** inner structure of MME, showing hornblende and needle-like apatites; **d** plagioclases included in the hornblende from the MME; **e** textural disequilibrium of plagioclase near the MME; **f** compositional and textural disequilibrium of plagioclase from the gneissic granite; also shown are the An contents; **g** microphotographs of the Dafangshen granite; **h** microphotograph of tourmaline from the Dafangshen pluton; **i** accessory minerals of the Hupiyu pluton. *Kfs* potash feldspar; *Pl* plagioclase; *Q* quartz; *Hb* hornblende; *Mag* magnetite; *Ttn* titanite; *Tur* tourmaline; *Ap* apatite

and mafic intrusions with metamorphic age of ca. 1.9 Ga (Yin and Nie 1996; Luo et al. 2004; Lu et al. 2006). These rocks are called the Liaohe Group in the eastern Liaoning Peninsula, which are further divided into the North Liaohe Group and the South Liaohe Group (Zhang 1984) by the Qinglongshan-Zaoerling ductile shear zones and faults (Li et al. 2005). The North Liaohe Group is characterized by the abundance of clastic and carbonate rocks, whereas the South Liaohe Group contains much more volcanic rocks (Fig. 7.2; Zhang and Yang 1988; Bai 1993; Lu et al. 1996; Bai and Dai 1998), including a volcanic-rich sequence in the lower part (the Lieryu and Gaojiayu Formations), a carbonate-rich sequence in the middle (the Dashiqiao Formation), and a pelitic sequence in the upper part (the Gaixian Formation). The well-known Paleoproterozoic boron deposits are hosted in the Lieryu Formation (~1300 m thick) that comprises metamorphosed boron-bearing volcano-sedimentary successions (Zhang 1984; Peng and Palmer 1995).

There are two groups of Paleoproterozoic granites in the Liaoji Belt, including dominantly metamorphosed gneissic granodiorite-granite with zircon ages from 2.2 to 2.1 Ga (Hao et al. 2004; Lu et al. 2006), and subordinate un-metamorphosed syenite-granite with zircon ages of ca. 1.84–1.87 Ga (Li et al. 2003; Cai et al. 2002; Lu et al. 2004). The latter are post-collisional, showing cross-cut contact with the metasedimentary and volcanic successions (the Liaohe Group). The gneissic granites typically contain foliated minerals such as hornblende and magnetite due to the

regional metamorphism (Hao et al. 2004). In this paper, we select five typical gneissic granite plutons for petrological and geochemical studies, trying to clarify their origin and geodynamic setting (Fig. 7.2). Petrological descriptions of these plutons are as below.

7.2 Petrological Descriptions of the Gneissic Granites

The Hupiyu gneissic pluton is composed mainly of 30 % microcline, 15 % perthite, 15 % plagioclase, 25 % quartz, and small amounts of biotite and hornblende, and accessory epidote, magnetite, zircon, apatite, and sphene. Lineation of hornblende, magnetite, and sphene forms the gneissic structure. No obvious compositional zoning is observed in plagioclase grains that have An contents of 0.47–1.14. Mafic dikes are present in the pluton, which have been metamorphosed into amphibolites (Fig. 7.3a). In addition, a few mafic microgranular enclaves (MME) of dioritic composition can be seen in the pluton.

The Hadabei monzonite pluton (Fig. 7.2) shows similar mineralogy to the Hupiyu pluton, with 40 % plagioclase, 25 % perthite, 30 % quartz, small amounts of hornblende and biotite, and accessory pyrrhotite, zircon, titanite, epidote, magnetite, and apatite. The pluton is also intruded by mafic dykes that have been transformed into amphibolites during the metamorphism. In addition, gabbroic diorite enclaves are common in the granite (Fig. 7.3b, c) and some plagioclase crystals are included by the hornblende in the MME (Fig. 7.3d). Plagioclases are characterized by compositional zoning (Fig. 7.3e, f): those far away from the MMEs show normal compositional zoning with An contents decreasing from core to rim, and those near the MMEs show reversal and complicated zoning textures (Fig. 7.3f).

The Muniuhe pluton (Fig. 7.2) is a gneissic hornblende biotite granite pluton, composed mainly of 35 % plagioclase, 15 % K-feldspar (perthite and small amounts of microline), 30 % quartz, 8 % biotite (partially altered to chlorite), and 7 % hornblende. Accessory minerals are zircon, sphene, and magnetite. The hornblende is euhedral. The biotite is foliated, and the plagioclase is kaolinised. Zonal texture of plagioclase is rare in the Muniuhe granite. Again, some dioritic dykes intruded into the granite.

The Dafangshen pluton is a gneissic K-feldspar granite pluton with metamorphic equilibrium textures (Fig. 7.3g), composed of 25 % microline, 15 % perthite, 5 % plagioclase, 40 % quartz, 10 % hornblende, and small amounts of biotite. Accessory minerals are tourmaline, zircon, zoisite, titanite, and magnetite. Banded distribution of hornblende, magnetite, and sphene forms the gneissic structure. The tourmaline is euhedral with obvious zonal structure (Fig. 7.3h).

The Simenzi pluton is a hornblende monzogranite pluton, composed mainly of 35 % microline, 25 % plagioclase, 25 % quartz and 10 % hornblende, and accessory zircon, sphene, and epidote. The hornblende is subhedral to euhedral. There are some dioritic dykes intruding into the granite.

7.3 Geochronology

The Liaoji Belt consists of Paleoproterozoic meta-volcano-sedimentary rocks, and granitic intrusions (Li et al. 2011). Previous studies have shown that the metasedimentary and volcanic rocks were formed at 2.2–2.0 Ga (Luo et al. 2004, 2008; Lu et al. 2006; Wan et al. 2006) and underwent greenschist to amphibolite facies metamorphism at ca. 1.9–1.93 Ga (Luo et al. 2004, 2008; Lu et al. 2006; Wan et al. 2006; Tam et al. 2011, 2012a, b). A few age data have been reported for the Paleoproterozoic gneissic granites. The gneissic granites in Haicheng and Kuandian have been dated at 2140 and 2070 Ma, respectively (Zhang and Yang 1988; Sun et al. 1993). The Qianzhuogou gneissic granite in the south of Liaonan was dated at 2160 Ma by Lu et al. (2005). Lu et al. (2004) reported a zircon U-Pb age of 2160 Ma for the Hupiyu gneissic granite.

Our new experimental data gained by LA-ICP-MS U-Pb zircon dating method shows that the Hupiyu gneissic granite was emplaced at 2183 Ma and the Hadabei pluton at 2173 Ma (Table 7.1), consistent with previous age data (Wu and Zheng 2004; Li and Zhao 2007). The Muniuhe pluton was formed at 2201 Ma and the Simenzi pluton at 2203 Ma. In summary, the gneissic granites in the JLJB were formed at ca. 2.17–2.20 Ga (Fig. 7.4). It should be stressed that we found inherited Archean zircons both in the gneissic granites and the amphibolite dykes intruding into the granites, such zircon inheritance was scarcely reported by previous researchers (Lu et al. 2004, 2005; Luo et al. 2004; Zhao et al. 2005; Li and Zhao 2007; Li et al. 2011). The ages of those inherited Archean zircons cluster at around 2.5 Ga and 2.7–2.8 Ga, in accordance with the ages of the two main Archean volcanisms within the NCC (Peuct et al. 1986; Liu et al. 1992; Wang et al. 1997; Geng et al. 2002; Zhao et al. 2002; Lu et al. 2004). These zircons of Archean ages suggest an Archean basement for the main source of the gneissic granites. The metamorphosed mafic dykes that intruded into the gneissic granites have been dated at 2159 Ma, indicating the intrusion happened shortly after the emplacement of the granites. U-Pb dating of the zircon overgrowth rims from the amphibolite yields an age of ca. 1.9 Ga, which coincides with the published metamorphic ages (Luo et al. 2004, 2008; Lu et al. 2006; Li et al. 2005; Li and Zhao 2007; Zhou et al. 2008; Tam et al. 2011) and is interpreted as the metamorphism age of the gneissic granites.

Table 7.1 In situ zircon U-Pb isotopic dating for the gneissic granites

Component/$\times 10^{-6}$			Th/U	Ratio				Age					
30 μm	Th	U		$^{206}Pb/^{238}U$	$^{206}Pb/^{238}U$	$^{207}Pb/^{235}U$	$^{207}Pb/^{235}U$	$^{206}Pb/^{238}U$	$^{206}Pb/^{238}U$	$^{207}Pb/^{235}U$	$^{207}Pb/^{235}U$	$^{207}Pb/^{206}Pb$	$^{207}Pb/^{206}Pb$
	ppm	pmm		Ratio	1sigma	Ratio	1sigma	Age (Ma)	1sigma	Age (Ma)	1sigma	Age (Ma)	1sigma
HD-2-1	103	107	1	0.37601	0.002	7.0823	0.0526	2057.6	9.2	2121.8	6.6	2184.3	9.1
HD-2-2	156	146	1.1	0.376342	0.004	7.0613	0.1051	2059.2	18.9	2119.2	13.2	2188.9	19.9
HD-2-3	110	104	1.1	0.357948	0.004	6.7274	0.097	1972.4	19.1	2076.2	12.7	2180.6	13.1
HD-2-4	97	123	0.8	0.362335	0.0018	6.7721	0.0377	1993.2	8.5	2082.1	4.9	2172.2	4.6
HD-2-5	110	100	1.1	0.365257	0.0061	6.9069	0.1106	2007	28.7	2099.5	14.2	2192.3	5.7
HD-2-6	74	83	0.9	0.365011	0.0024	6.8603	0.0501	2005.9	11.5	2093.5	6.5	2180.6	4.6
HD-2-7	37	50	0.7	0.366977	0.0025	6.9404	0.0515	2015.2	11.8	2103.8	6.6	2191.1	5.6
HD-2-8	87	130	0.7	0.362557	0.0024	6.7932	0.0465	1994.3	11.5	2084.8	6.1	2175.9	3.5
HD-2-9	40	54	0.7	0.360724	0.0022	6.8111	0.0489	1985.6	10.6	2087.2	6.4	2188.0	5.7
HD-2-10	52	61	0.9	0.366016	0.0025	6.8979	0.0481	2010.6	11.6	2098.4	6.2	2184.9	5.4
HD-2-11	33	44	0.8	0.379136	0.0036	7.0991	0.0827	2072.2	16.7	2123.9	10.4	2173.2	9.1
HD-2-12	51	58	0.9	0.374443	0.0021	7.0099	0.0539	2050.3	9.7	2112.7	6.8	2173.2	9.3
HD-2-13	73	67	1.1	0.36889	0.0019	6.8969	0.0369	2024.2	9	2098.3	4.7	2172.2	3.6
HD-2-14	57	62	0.9	0.383221	0.0035	7.1764	0.0871	2091.3	16.5	2133.6	10.8	2173.2	9.4
HD-2-15	90	85	1.1	0.384555	0.0018	7.189	0.0397	2097.5	8.6	2135.1	4.9	2172.2	6.5
HD-2-16	48	53	0.9	0.397158	0.0056	7.446	0.1074	2155.9	25.6	2166.5	12.9	2176.2	9.3
HD-2-17	62	62	1	0.384441	0.0033	7.2219	0.0644	2097	15.2	2139.2	8	2179.9	7.4
HD-2-18	62	65	1	0.364533	0.0058	6.8571	0.1157	2003.6	27.2	2093.1	15	2181.2	8.5
HD-2-19	62	65	1	0.386326	0.0078	7.2305	0.1467	2105.8	36.1	2140.3	18.1	2173.2	9.1
HD-2-20	46	56	0.8	0.386781	0.0043	7.2364	0.0814	2107.9	19.7	2141	10	2171.9	4.2
HD-2-21	31	44	0.7	0.378658	0.0058	7.0928	0.11	2070	27.1	2123.1	13.8	2175.9	9.9
HD-2-22	59	70	0.8	0.366921	0.0077	6.8706	0.1326	2014.9	36.1	2094.9	17.1	2175.9	8.3
HD-2-23	127	113	1.1	0.383248	0.003	7.1738	0.0582	2091.4	13.9	2133.2	7.2	2173.2	4.6
HD-2-24	93	95	1	0.380753	0.0028	7.1345	0.0531	2079.8	12.8	2128.4	6.6	2175.9	4.6
HD-2-25	97	102	1	0.365976	0.0024	6.8656	0.0483	2010.4	11.3	2094.2	6.2	2176.9	4.6
HD-2-26	72	77	0.9	0.378709	0.0031	7.1076	0.0609	2070.3	14.3	2125	7.6	2177.5	5.6
HD-2-27	87	93	0.9	0.381092	0.0026	7.1538	0.0511	2081.4	12.2	2130.8	6.4	2188.9	5.6
HD-2-28	114	114	1	0.375289	0.0033	7.0709	0.0654	2054.2	15.5	2120.4	8.2	2184.3	0.8
HD-2-29	99	106	0.9	0.362595	0.005	6.8371	0.1013	1994.5	23.6	2090.5	13.1	2187.0	8.6
HD-2-30	22	134	0.2	0.348026	0.0102	6.601	0.1985	1925.2	48.9	2059.5	26.5	2196.0	12.5
HP-1-1	168	176	1	0.38062	0.0056	7.1302	0.1015	2079.2	26.3	2127.8	12.7	2175.9	11.3
HP-1-3	152	153	1	0.37865	0.0022	7.1325	0.0473	2070	10.3	2128.1	5.9	2184.9	0.8

(continued)

Table 7.1 (continued)

Component/$\times 10^{-6}$			Th/U	Ratio				Age					
30 μm	Th	U		$^{206}Pb/^{238}U$	$^{206}Pb/^{238}U$	$^{207}Pb/^{235}U$	$^{207}Pb/^{235}U$	$^{206}Pb/^{238}U$	$^{206}Pb/^{238}U$	$^{207}Pb/^{235}U$	$^{207}Pb/^{235}U$	$^{207}Pb/^{206}Pb$	$^{207}Pb/^{206}Pb$
	ppm	pmm		Ratio	1sigma	Ratio	1sigma	Age (Ma)	1sigma	Age (Ma)	1sigma	Age (Ma)	1sigma
HP-1-4	31	50	0.6	0.3784	0.0028	7.095	0.0543	2068.8	13.3	2123.4	6.8	2177.5	9.3
HP-1-5	37	55	0.7	0.38753	0.0025	7.2494	0.0513	2111.4	11.7	2142.6	6.3	2173.2	6.8
HP-1-6	45	53	0.9	0.3825	0.0058	7.199	0.1122	2087.9	27.2	2136.4	13.9	2183.6	11.9
HP-1-7	95	105	0.9	0.37729	0.0028	7.0837	0.0592	2063.6	12.9	2122	7.4	2188.9	6.2
HP-1-8	80	104	0.8	0.38136	0.003	7.1642	0.0593	2082.7	14	2132.1	7.4	2179.9	5.6
HP-1-9	65	74	0.9	0.38791	0.0053	7.2808	0.111	2113.1	24.4	2146.5	13.6	2188.9	11.1
HP-1-10	96	104	0.9	0.39777	0.0052	7.486	0.0563	2158.8	24	2171.3	6.7	2183.6	20.4
HP-1-11	95	109	0.9	0.3857	0.0038	7.2585	0.0808	2102.9	17.4	2143.7	9.9	2183.0	11.4
HP-1-12	131	137	1	0.40724	0.0028	7.6978	0.0572	2202.3	13	2196.3	6.7	2190.4	4.2
HP-1-14	71	86	0.8	0.39649	0.0024	7.4251	0.0474	2152.9	10.9	2164	5.7	2175.9	4.9
HP-1-15	40	62	0.7	0.39157	0.0063	7.3859	0.1198	2130.1	29.2	2159.3	14.5	2187.4	15.1
HP-1-16	79	76	1	0.40826	0.0185	7.562	0.324	2207	84.5	2180.4	38.4	2166.7	9.7
HP-1-17	88	90	1	0.38247	0.0052	7.1666	0.1182	2087.8	24.1	2132.4	14.7	2175.9	9.9
HP-1-18	31	45	0.7	0.38975	0.0043	7.3218	0.2315	2121.7	19.9	2151.5	28.3	2188.9	38.9
HP-1-19	97	97	1	0.38381	0.0107	7.2137	0.212	2094.1	49.8	2138.2	26.2	2179.9	11.9
HP-1-20	97	99	1	0.39497	0.0039	7.3768	0.0785	2145.8	18.2	2158.2	9.5	2169.4	7.7
HP-1-21	60	71	0.8	0.38727	0.0039	7.1797	0.0792	2110.2	18.1	2134	9.8	2166.7	7.4
HP-1-22	101	120	0.9	0.3961	0.0034	7.3448	0.0678	2151	15.7	2154.3	8.2	2166.7	7.6
HP-1-23	89	109	0.8	0.41435	0.0034	7.7489	0.0709	2234.8	15.6	2202.3	8.2	2172.2	12.2
HP-1-25	66	103	0.6	0.39129	0.0025	7.3017	0.0504	2128.8	11.6	2149	6.2	2168.5	3.6
HP-1-26	108	123	0.9	0.38057	0.0053	7.1638	0.1046	2079	24.7	2132	13	2183.3	7.6
HP-1-27	122	142	0.9	0.39396	0.0036	7.4201	0.0687	2141.1	16.6	2163.4	8.3	2184.3	0.9
HP-1-28	74	117	0.6	0.39185	0.0027	7.3768	0.0559	2131.4	12.5	2158.2	6.8	2183.0	6.9
HP-1-29	78	130	0.6	0.39211	0.0029	7.3731	0.0555	2132.6	13.3	2157.7	6.7	2183.3	5.1
MN-6-2	92	122	0.8	0.38311	0.0061	7.2438	0.1208	2090.8	28.6	2141.9	14.9	2190.7	7.3
MN-6-3	88	95	0.9	0.38587	0.003	7.3303	0.0577	2103.7	13.8	2152.5	7	2199.1	7.7
MN-6-4	94	96	1	0.37955	0.0036	7.126	0.1631	2074.2	16.8	2127.3	20.4	2188.9	24.2
MN-6-5	58	205	0.3	0.38012	0.0025	9.0303	0.0687	2076.9	11.9	2341.1	7.0	2579.3	6.9
MN-6-7	68	81	0.8	0.38058	0.0033	7.2253	0.0677	2079	15.3	2139.6	8.4	2197.8	7.3
MN-6-8	85	84	1	0.40105	0.0041	7.6002	0.0839	2173.9	19	2184.9	9.9	2194.8	8.0
MN-6-9	232	248	0.9	0.35614	0.0034	7.5034	0.1165	1963.8	16.3	2173.4	13.9	2376.9	15.4
MN-6-13	36	63	0.6	0.37665	0.0048	7.156	0.0964	2060.6	22.3	2131	12	2199.7	9.7

(continued)

Table 7.1 (continued)

Component/×10^{-6}			Th/U	Ratio				Age					
30 μm	Th	U		$^{206}Pb/^{238}U$	$^{206}Pb/^{238}U$	$^{207}Pb/^{235}U$	$^{207}Pb/^{235}U$	$^{206}Pb/^{238}U$	$^{206}Pb/^{238}U$	$^{207}Pb/^{235}U$	$^{207}Pb/^{235}U$	$^{207}Pb/^{206}Pb$	$^{207}Pb/^{206}Pb$
	ppm	pmm		Ratio	1sigma	Ratio	1sigma	Age (Ma)	1sigma	Age (Ma)	1sigma	Age (Ma)	1sigma
MN-6-15	65	83	0.8	0.3822	0.0039	7.2569	0.0777	2086.6	18.2	2143.5	9.6	2198.5	11.4
MN-6-16	34	59	0.6	0.36895	0.0057	7.012	0.1177	2024.4	26.8	2113	14.9	2199.7	9.3
MN-6-17	103	107	1	0.36921	0.0047	7.0431	0.0936	2025.7	22.1	2116.9	11.8	2206.5	6.8
MN-6-18	54	83	0.7	0.38117	0.0085	7.23	0.1558	2081.7	39.7	2140.2	19.2	2198.2	11.1
MN-6-19	190	254	0.8	0.32966	0.0060	7.1472	0.0628	1836.7	29.2	2129.9	7.8	2427.8	17.4
MN-6-20	54	74	0.7	0.38243	0.003	7.2776	0.0628	2087.6	13.8	2146.1	7.7	2202.2	7.7
MN-6-21	23	38	0.6	0.3808	0.0068	7.2217	0.1654	2080	31.8	2139.2	20.4	2195.4	20.4
MN-6-22	73	104	0.7	0.36891	0.0098	7.0747	0.1966	2024.3	46.1	2120.9	24.7	2216.7	11.1
MN-6-23	95	105	0.9	0.38476	0.0081	7.3037	0.1788	2098.5	37.6	2149.3	21.9	2198.2	9.9
MN-6-24	31	48	0.6	0.37664	0.0077	7.1484	0.1658	2060.6	35.9	2130.1	20.7	2198.2	14.8
MN-6-25	100	115	0.9	0.40095	0.0044	7.6424	0.0943	2173.4	20.2	2189.9	11.1	2205.2	9.6
MN-6-27	13	20	0.6	0.38206	0.0156	7.2557	0.3212	2085.9	72.7	2143.4	39.5	2195.4	12.0
MN-6-28	69	69	1	0.38313	0.0027	7.2747	0.0555	2090.9	12.7	2145.7	6.8	2198.5	6.6
MN-6-29	142	108	1.3	0.39435	0.0067	7.5213	0.1366	2143	31.1	2175.5	16.3	2205.9	8.0
MN-6-30	107	92	1.2	0.3865	0.0058	7.3614	0.1138	2106.6	26.8	2156.3	13.8	2205.6	8.5
SM-1-1	212	258	0.8	0.33405	0.0032	7.4993	0.0884	1858.0	15.6	2172.9	10.6	2484.9	9.7
SM-1-2	275	351	0.8	0.28189	0.0032	7.5642	0.1068	1600.9	15.8	2180.6	12.7	2783.0	20.4
SM-1-5	52	64	0.8	0.388	0.0046	7.3765	0.0933	2113.5	21.3	2158.1	11.3	2201.5	10.6
SM-1-6	47	69	0.7	0.38806	0.0040	7.3832	0.0807	2113.8	18.8	2158.9	9.8	2202.8	5.6
SM-1-7	302	287	1.0	0.33138	0.0040	7.5057	0.1134	1845.0	19.5	2173.7	13.5	2501.9	11.1
SM-1-8	107	148	0.7	0.39855	0.0169	7.5511	0.3511	2162.4	78	2179.1	41.7	2194.8	7.4
SM-1-10	145	143	1	0.38787	0.0042	7.4333	0.0999	2112.9	19.6	2165	12	2214.5	7.7
SM-1-11	6	265	0	0.32835	0.0018	6.2716	0.0626	1830.4	8.7	2014.5	8.7	2205.6	11.1
SM-1-13	136	163	0.8	0.38145	0.0042	7.2821	0.0887	2083	19.8	2146.6	10.9	2207.1	5.4
SM-1-14	39	57	0.7	0.37393	0.007	7.1042	0.1108	2047.8	32.6	2124.6	13.9	2202.2	19.0
SM-1-15	38	44	0.9	0.37387	0.0167	7.1397	0.2156	2047.6	78.6	2129	26.9	2213.9	80.2
SM-1-16	45	56	0.8	0.39203	0.0188	7.4385	0.3365	2132.2	87.2	2165.6	40.5	2198.5	17.9
SM-1-17	59	73	0.8	0.38639	0.0174	7.2986	0.4113	2106.1	81.1	2148.6	50.4	2188.6	20.5
SM-1-19	119	155	0.8	0.3877	0.0043	7.4067	0.0892	2112.2	19.9	2161.8	10.8	2209.3	5.6
SM-1-20	100	136	0.7	0.40806	0.0116	7.7928	0.2731	2206	53.2	2207.4	31.5	2207.1	12.7
SM-1-21	207	267	0.7	0.36318	0.0112	7.9811	0.2758	1997.2	53.1	2228.9	31.2	2449.1	33.2
SM-1-23	40	51	0.8	0.36798	0.0089	7.0206	0.2069	2019.9	42.1	2114	26.2	2205.9	14.0

(continued)

Table 7.1 (continued)

Component/×10^{-6}			Th/U	Ratio				Age					
30 μm	Th	U		$^{206}Pb/^{238}U$	$^{206}Pb/^{238}U$	$^{207}Pb/^{235}U$	$^{207}Pb/^{235}U$	$^{206}Pb/^{238}U$	$^{206}Pb/^{238}U$	$^{207}Pb/^{235}U$	$^{207}Pb/^{235}U$	$^{207}Pb/^{206}Pb$	$^{207}Pb/^{206}Pb$
	ppm	pmm		Ratio	1sigma	Ratio	1sigma	Age (Ma)	1sigma	Age (Ma)	1sigma	Age (Ma)	1sigma
SM-1-24	279	349	0.8	0.30652	0.0062	7.8182	0.1218	1723.6	30.7	2210.3	14.0	2712.7	36.9
SM-1-26	226	270	0.8	0.33777	0.0096	7.7597	0.2229	1875.9	46.1	2203.6	25.8	2525.6	25.6
SM-1-27	57	68	0.8	0.37929	0.0053	7.1906	0.1036	2073	24.8	2135.3	12.8	2196.0	5.7
SM-1-28	57	73	0.8	0.38772	0.0029	7.3878	0.0586	2112.3	13.5	2159.5	7.1	2205.6	-0.9
SM-1-29	27	45	0.6	0.37515	0.004	7.093	0.1199	2053.6	18.9	2123.2	15	2191.1	29.6
HP-9-02	2056	1133	1.81	0.36318	0.0051	6.792	0.117	1997	24	2085	15	2172	14
HP-9-03	13716	2911	4.71	0.36769	0.0052	6.912	0.119	2019	24	2100	15	2181	14
HP-9-06	*76*	*208*	*0.36*	*0.36755*	*0.0052*	*5.916*	*0.106*	*2018*	*25*	*1966*	*16*	*1907*	*15*
HP-9-07	*593*	*626*	*0.95*	*0.37312*	*0.0059*	*6.312*	*0.206*	*2044*	*28*	*2020*	*29*	*1996*	*66*
HP-9-10	1142	987	1.16	0.40078	0.0057	7.524	0.133	2173	26	2176	16	2178	14
HP-9-11	1749	1168	1.50	0.36773	0.0052	6.844	0.121	2019	24	2091	16	2164	14
HP-9-12	606	538	1.13	0.44459	0.0063	8.309	0.148	2371	28	2265	16	2171	14
HP-9-14	482	434	1.11	0.35517	0.0051	6.591	0.119	1959	24	2058	16	2158	15
HP-9-15	1259	1070	1.18	0.36503	0.0052	6.708	0.120	2006	24	2074	16	2141	14
HP-9-16	1215	1046	1.16	0.37457	0.0053	6.983	0.127	2051	25	2109	16	2166	15
HP-9-20	80	966	0.08	0.46455	0.0065	10.702	0.190	2460	28	2498	16	2529	19
HP-9-21	684	164	4.18	0.36209	0.0053	6.026	0.115	1992	25	1980	17	1966	16
HP-9-22	1493	441	3.39	0.38343	0.0055	6.870	0.127	2092	26	2095	16	2097	15
HP-9-23	836	839	1.00	0.38144	0.0055	7.022	0.130	2083	25	2114	16	2144	15
HP-9-25	348	915	0.38	0.38378	0.0055	6.951	0.129	2094	26	2105	16	2116	15
HP-9-30	1368	771	1.78	0.39731	0.0057	7.374	0.139	2157	26	2158	17	2159	15
HP-9-32	324	343	0.94	0.42185	0.0061	7.730	0.148	2269	28	2200	17	2136	16
HP-9-35	1765	1632	1.08	0.34916	0.005	6.525	0.125	1931	24	2049	17	2171	16
HP-9-37	1463	884	1.65	0.30702	0.0045	5.257	0.102	1726	22	1862	17	2017	16
HP-9-38	405	349	1.16	0.39281	0.0057	7.168	0.142	2136	27	2133	18	2129	16
HP-9-40	13	57	0.23	0.36077	0.0057	6.108	0.140	1986	27	1991	20	1997	20

HD-2: the Hadabei granite;
HP-1: the Hupiyu granite;
MN-6: the Muniuhe granite;
SM-1: the Simenzi granite;
HP-9: the mafic dyke

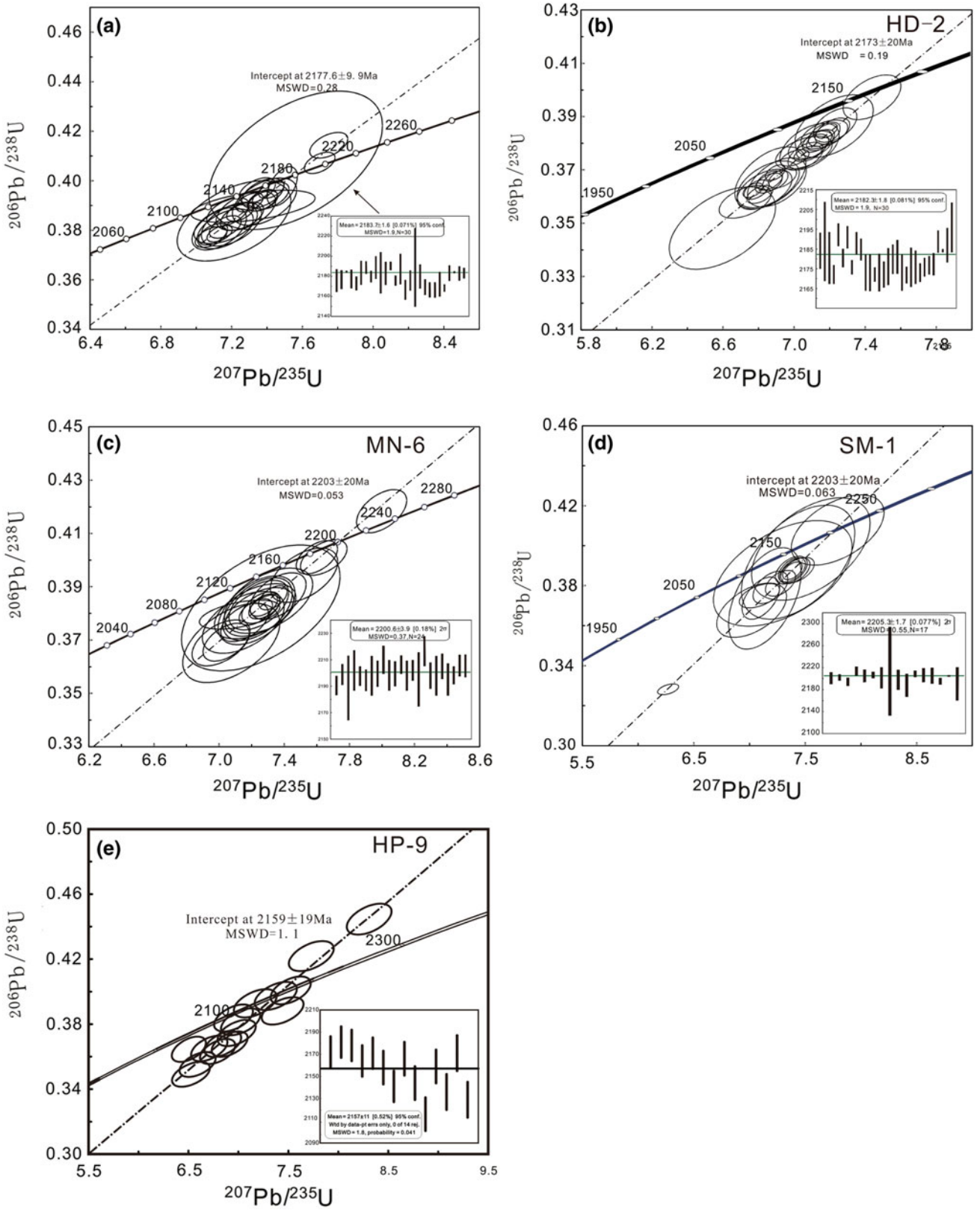

Fig. 7.4 Zircon U-Pb isotope concordia diagrams; **a** the Hupiyu granite; **b** the Hadabei granite; **c** the Muniuhe granite; **d** the Simenzi granite; **e** mafic dyke

7.4 A-type Granites?

The gneissic granites have been regarded as A-type granite in previous studies (Wu and Zheng 2004; Hao et al. 2004; Zhao et al. 2005), mainly based on limited data plotted in some geochemical diagrams such as Zr + Nb + Ce + Y versus FeO/MgO.

In this paper, we suggest that the gneissic granites are calc-alkaline I-type granites based on the following lines of evidences. (1) A-type granite commonly formed in an anorogenic setting and shows water-deficient and alkaline characteristics (e.g., Whalen et al. 1987). Hornblendes in A-type granites, if any, are generally Na-rich alkaline ones (Whalen et al. 1987). We saw no alkali hornblende or sodium hornblende in these gneissic granite samples, rather, the hornblendes within these rocks are mainly euhedral calcium hornblendes and magnesiohornblendes (Figs. 7.3i, c and 7.5; Table 7.2). (2) Lots of titanites and magnetites occur in these granites (Fig. 7.3i), which, along with the abundance of calcium hornblende and some MMEs (Fig. 7.3b), suggest a calc-alkaline, H_2O-rich, and high fO_2 affinity of the parental magma, typical of I-type granites. (3) The major elements show medium potassium calc-alkaline features (Fig. 7.6). These granites are enriched in LILEs, such as K, Rb, Sr, and Cs, and depleted in some HFSEs that are otherwise enriched in A-type granites, such as Nb, Ta, and Th. The chondrite-normalized REE patterns of these granites are different from those of A-type granites which are commonly characterized by significant negative Eu anomalies and tetrad effects. (4) Negative Ba anomalies are not so significant as in many A-types (Whalen et al. 1987), which may be caused by the enrichment of H_2O in the magma system. Because water-saturated felsic magma tends to show high oxygen fugacity and high internal water pressure due to exsolution of discrete vapor phases and the thermal breakdown of H_2O (Bonin 1990). As a consequence, alkali feldspar fractionation and, thus, negative Ba anomalies, are reduced. In addition, the contents of Fe and Ti are also lower than those of typical A-type granites, which may also be caused by the H_2O-enrichment in the magma system, because titanomagnetite and Nb-Mn ilmenite precipitate in an early stage, decreasing the contents of Fe and Ti in residual magma (Bonin 1990). These data suggest that the Paleoproterozoic gneissic granites could be basically water-enriched I-type granites (Tables 7.3 and 7.4).

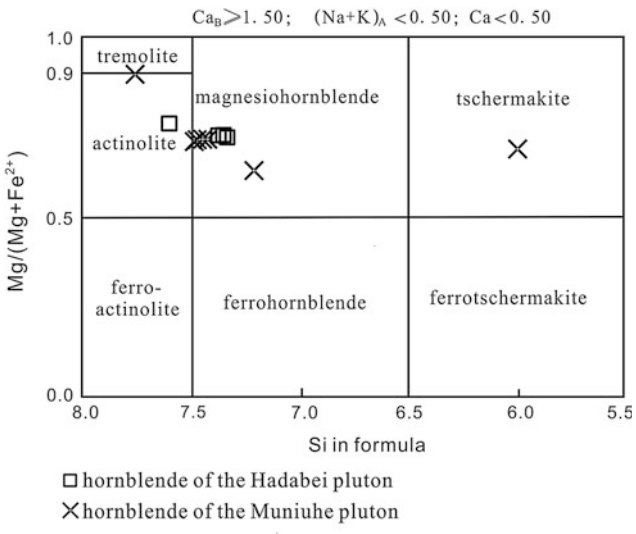

Fig. 7.5 Classfication diagram of hornblende from the Hadabei and Muniuhe granites (after Leake et al. 1997)

However, some samples from the Dafangshen pluton show A-type features. As shown in Fig. 7.7, these samples have significant negative Eu anomalies (Eu/Eu* = 0.1), slight REE tetrad effect ($TE_{1,3}$ = 0.12–0.21) and lower Zr/Hf ratios (30.5–33.7) than in normal granites (35–40, Jahn et al. 2001; Chen et al. 2014). We suggest that the A-type-like characteristics are attributable to the highly evolved nature of the pluton as shown by the high SiO_2 contents (76.7–77.1 wt%), which could have been caused by the high boron contents of the pluton, because tourmaline (texturally in equilibrium with other rock-forming minerals) is common in this pluton (Fig. 7.3h). The B-rich feature of the Dafangshen granite (>1 wt% boron for the crystallization of tourmaline; Lukkari and Holtz 2007) could have lowered the solidus temperature and viscosity of the magma system (Chen et al. 2014), and thus prolong the process of magma evolution and strengthen the melt-rock interaction, leading to high silica, non-CHARAC characteristics (e.g., low Zr/Hf ratios) and the slight REE tetrad effect of the pluton (Bau 1996; Chen et al. 2014). This is also supported by the occurrence of extremely Ab-rich plagioclase in the Dafangshen pluton (with Ab = 71.1–98.3), a feature typical of highly evolved (A-type) granites (Whalen et al. 1987). The Ab-rich feature could have been related with addition of boron in the magma system, which was proved to shift the ternary minimum composition towards the Ab apex in the phase relations of Ab-Or-Qtz (Manning 1981).

7.5 Role of Magma Mixing/Mingling

According to the petrography and geochemical characteristics of these gneissic granites, we suggest that they formed through a mingling/mixing process between dominant crustal melts and subordinate mantle-derived mafic magmas. This is supported by the following lines of evidence.

First, MMEs are common in the gneissic granites (Fig. 7.3b, c). Although MMEs have been suggested as early crystallized mineral cumulates from magma chamber (Noyes et al. 1983), or as residual phases after partial melting of source rocks (White et al. 1999; Chappell et al. 2000), we

Table 7.2 Microprobe analysis for representative hornblende from the Liao-Ji gneissic granites

Pluton	Hadabei				Muniuhe							
Spot no.	HD-7.1	HD-7.2	HD-7.3	HD-7.4	MN-4.1	MN-4.2	MN-4.3	MN-4.4	MN-4.5	MN-4.6	MN-4.7	MN-4.8
SiO_2	54.8	51.84	52.63	52.1	52.72	30.47	53.36	53.3	52.83	56.82	50.06	42.59
TiO_2	0.1	0.35	0.16	0.15	0.29	37.62	0.06	0.17	0.08	0.03	0.43	1.89
Al_2O_3	1.49	3.1	2.95	3.03	2.66	1.42	2.5	2.85	2.24	0.33	3.1	12.72
Cr_2O_3	0	0.07	0.02	0.03	0.05	0.12	0.06	0.17	0	0.09	0.01	0.08
Fe_2O_3	4.87	4.87	4.87	4.87	4.87	4.87	4.87	4.87	4.87	4.87	4.87	4.87
FeO	9.88	11.08	11.13	10.97	10.18	0.31	10.68	10.29	10.66	4.23	16.47	10.27
MnO	0.33	0.37	0.34	0.36	0.18	0.01	0.25	0.23	0.19	0.24	0.44	0.11
MgO	18.36	16.75	17.25	17.15	17.17	0.04	16.93	16.87	17.36	22.9	13.23	15.49
CaO	12.35	12.37	12.28	12.25	13.27	30.17	13.32	13.16	13.39	12.48	12.1	11.85
Na_2O	0.42	0.82	0.84	0.87	0.29	0	0.3	0.36	0.32	0.11	0.56	2.52
K_2O	0.1	0.23	0.2	0.22	0.14	0	0.13	0.15	0.12	0.07	0.33	0.96
Totals	102.7	101.86	102.68	102.01	101.82	105.06	102.46	102.42	102.06	102.17	101.61	103.36
Oxygens	23	23	23	23	23	23	23	23	23	23	23	23
Si	7.525	7.27	7.308	7.286	7.349	4.426	7.401	7.381	7.367	7.63	7.226	5.986
Ti	0.01	0.037	0.017	0.016	0.03	4.11	0.006	0.018	0.008	0.003	0.047	0.2
Al	0.241	0.513	0.483	0.5	0.437	0.243	0.409	0.465	0.368	0.052	0.528	2.108
Cr	0	0.008	0.002	0.003	0.006	0.014	0.007	0.019	0	0.01	0.001	0.009
Fe^{3+}	0.504	0.514	0.509	0.513	0.511	0.533	0.509	0.508	0.512	0.493	0.53	0.516
Fe^{2+}	1.135	1.299	1.292	1.283	1.187	0.038	1.239	1.192	1.243	0.475	1.988	1.207
Mn	0.038	0.044	0.04	0.043	0.021	0.001	0.029	0.027	0.022	0.027	0.054	0.013
Mg	3.757	3.501	3.57	3.574	3.567	0.009	3.5	3.482	3.608	4.583	2.846	3.245
Ca	1.817	1.859	1.827	1.836	1.982	4.696	1.98	1.953	2.001	1.796	1.871	1.785
Na	0.112	0.223	0.226	0.236	0.078	0	0.081	0.097	0.087	0.029	0.157	0.687
K	0.018	0.041	0.035	0.039	0.025	0	0.023	0.027	0.021	0.012	0.061	0.172
Sum	15.157	15.308	15.309	15.328	15.195	14.071	15.183	15.167	15.238	15.11	15.307	15.927
Mg#	0.77	0.73	0.73	0.74	0.75	0.19	0.74	0.74	0.74	0.91	0.59	0.73

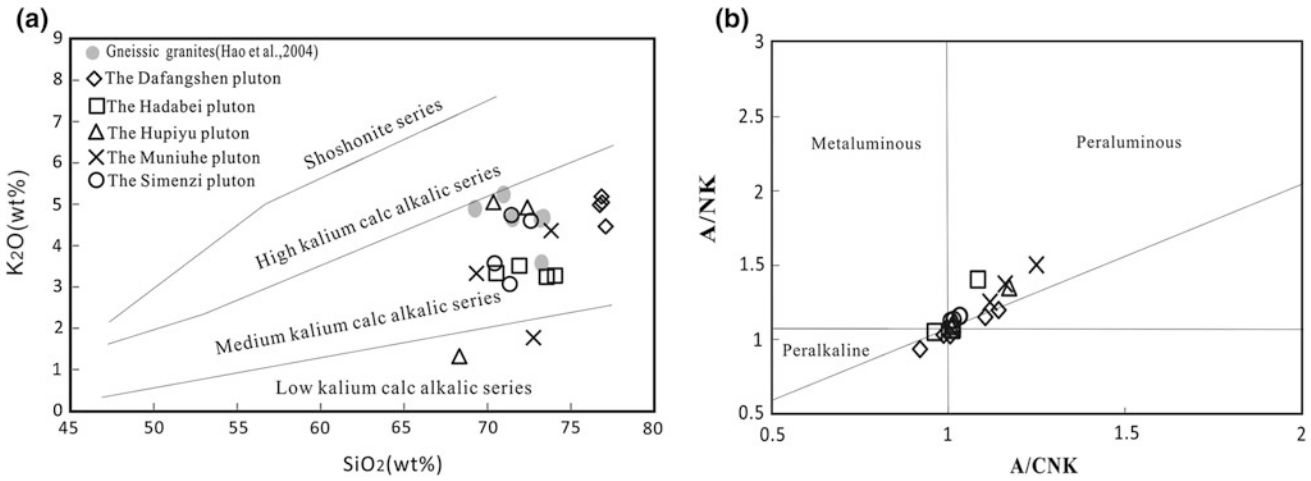

Fig. 7.6 **a** K_2O-SiO_2 diagram (after Peccerillo and Taylor 1976) and **b** A/NK-A/CNK diagram for the granites

Table 7.3 Microprobe analysis for representative plagioclase from the gneissic granites

Pluton	Hupiyu						Hadabei					
Spot no.	HP-1.3	HP-1.4	HP-1.5	HP-6.1	HP-6.2	HP-6.3	HD-2.1	HD-2.2	HD-2.3	HD-2.4	HD-1.1	HD-1.2
SiO_2	67.86	65.73	66.49	67.93	66.56	69.08	59.55	59.46	62.10	58.13	58.70	58.82
TiO_2	0.07	0.04	0.00	0.04	0.02	0.02	0.08	0.06	0.00	0.00	0.00	0.05
Al_2O_3	19.01	20.54	20.29	20.82	20.58	19.37	24.64	24.47	22.47	25.31	25.50	24.78
Cr_2O_3	0.07	0.00	0.03	0.00	0.01	0.02	0.02	0.00	0.07	0.04	0.00	0.00
Fe_2O_3	0.00	0.00	0.00	0.00	0.00	0.00	0.00	0.00	0.00	0.00	0.00	0.00
FeO	0.00	0.00	0.00	0.00	0.00	0.00	0.00	0.00	0.00	0.00	0.00	0.00
MnO	0.00	0.00	0.00	0.05	0.00	0.00	0.01	0.00	0.00	0.06	0.00	0.00
MgO	0.00	0.01	0.00	0.00	0.00	0.01	0.01	0.00	0.00	0.00	0.01	0.00
CaO	0.23	1.30	1.26	1.36	1.32	0.11	6.08	6.62	3.95	6.87	6.88	6.78
Na_2O	11.03	12.37	11.97	11.19	12.21	12.57	8.83	8.42	10.16	7.94	8.14	8.15
K_2O	0.08	0.30	0.08	0.12	0.19	0.06	0.53	0.45	0.56	0.49	0.38	0.47
Total	98.35	100.29	100.12	101.51	100.89	101.24	99.75	99.48	99.31	98.84	99.61	99.05
Si	3.01	2.90	2.92	2.93	2.91	2.99	2.67	2.67	2.78	2.63	2.64	2.66
Ti	0.00	0.00	0.00	0.00	0.00	0.00	0.00	0.00	0.00	0.00	0.00	0.00
Al	0.99	1.07	1.05	1.06	1.06	0.99	1.30	1.30	1.19	1.35	1.35	1.32
Cr	0.00	0.00	0.00	0.00	0.00	0.00	0.00	0.00	0.00	0.00	0.00	0.00
Fe^{3+}	0.00	0.00	0.00	0.00	0.00	0.00	0.00	0.00	0.00	0.00	0.00	0.00
Fe^{2+}	0.00	0.00	0.00	0.00	0.01	0.00	0.01	0.01	0.01	0.01	0.01	0.01
Mn	0.00	0.00	0.00	0.00	0.00	0.00	0.00	0.00	0.00	0.00	0.00	0.00
Mg	0.00	0.00	0.00	0.00	0.00	0.00	0.00	0.00	0.00	0.00	0.00	0.00
Ca	0.01	0.06	0.06	0.06	0.06	0.01	0.29	0.32	0.19	0.33	0.33	0.33
Na	0.95	1.06	1.02	0.94	1.04	1.06	0.77	0.73	0.88	0.70	0.71	0.71
K	0.01	0.02	0.00	0.01	0.01	0.00	0.03	0.03	0.03	0.03	0.02	0.03
An	1.14	5.37	5.45	6.26	5.60	0.47	26.79	29.56	17.21	31.47	31.17	30.68
Ab	98.34	93.13	94.18	93.05	93.41	99.25	70.46	68.03	79.89	65.88	66.76	66.79
Or	0.52	1.50	0.37	0.70	0.99	0.28	2.75	2.41	2.90	2.65	2.07	2.53

Pluton	Hadabei											Dafangshen
Spot no.	HD-1.3	HD-1.4	HD-1.5	HD-1.6	HD-7.1	HD-7.2	HD-7.3	HD-7.4	HD-7.5	HD-7.6	HD-7.7	DF-8.1
SiO_2	57.61	58.40	58.66	59.63	59.26	57.97	63.46	59.43	64.43	56.60	62.87	59.82
TiO_2	0.01	0.04	0.00	0.01	0.03	0.00	0.04	0.01	0.03	0.00	0.00	0.00
Al_2O_3	25.61	25.60	24.88	25.02	24.42	25.48	22.37	24.96	22.69	27.16	22.67	25.48

(continued)

Table 7.3 (continued)

Pluton	Hadabei											Dafangshen
Spot no.	HD-1.3	HD-1.4	HD-1.5	HD-1.6	HD-7.1	HD-7.2	HD-7.3	HD-7.4	HD-7.5	HD-7.6	HD-7.7	DF-8.1
Cr_2O_3	0.03	0.00	0.02	0.00	0.00	0.00	0.01	0.00	0.00	0.01	0.00	0.00
Fe_2O_3	0.00	0.00	0.00	0.00	0.18	0.09	0.21	0.17	0.18	0.15	0.14	0.00
FeO	0.00	0.00	0.00	0.00	0.00	0.00	0.00	0.00	0.00	0.00	0.00	0.00
MnO	0.00	0.00	0.03	0.01	0.04	0.00	0.03	0.01	0.01	0.00	0.01	0.02
MgO	0.01	0.04	0.01	0.01	0.03	0.00	0.01	0.02	0.00	0.03	0.01	0.02
CaO	7.65	7.55	7.16	5.89	6.63	7.54	3.85	6.62	3.97	8.83	4.13	6.25
Na_2O	7.84	7.90	8.40	8.57	7.94	7.42	9.26	7.87	7.98	7.38	9.26	9.10
K_2O	0.38	0.42	0.34	0.48	0.72	0.47	0.27	0.63	0.36	0.26	0.54	0.38
Total	99.14	99.95	99.50	99.62	99.25	98.98	99.51	99.73	99.66	100.42	99.62	101.07
Si	2.61	2.62	2.64	2.67	2.67	2.63	2.82	2.67	2.84	2.54	2.80	2.65
Ti	0.00	0.00	0.00	0.00	0.00	0.00	0.00	0.00	0.00	0.00	0.00	0.00
Al	1.37	1.35	1.32	1.32	1.30	1.36	1.17	1.32	1.18	1.44	1.19	1.33
Cr	0.00	0.00	0.00	0.00	0.00	0.00	0.00	0.00	0.00	0.00	0.00	0.00
Fe^{3+}	0.00	0.00	0.00	0.00	0.01	0.00	0.01	0.01	0.01	0.01	0.01	0.00
Fe^{2+}	0.01	0.01	0.01	0.00	0.00	0.00	0.00	0.00	0.00	0.00	0.00	0.00
Mn	0.00	0.00	0.00	0.00	0.00	0.00	0.00	0.00	0.00	0.00	0.00	0.00
Mg	0.00	0.00	0.00	0.00	0.00	0.00	0.00	0.00	0.00	0.00	0.00	0.00
Ca	0.37	0.36	0.35	0.28	0.32	0.37	0.18	0.32	0.19	0.43	0.20	0.30
Na	0.69	0.69	0.73	0.74	0.70	0.65	0.80	0.68	0.68	0.64	0.80	0.78
K	0.02	0.02	0.02	0.03	0.04	0.03	0.02	0.04	0.02	0.02	0.03	0.02
An	34.32	33.80	31.45	26.85	30.34	35.06	18.37	30.64	21.10	39.28	19.20	27.00
Ab	63.64	63.97	66.73	70.59	65.69	62.36	80.12	65.90	76.54	59.33	77.88	71.09
Or	2.04	2.23	1.82	2.56	3.97	2.59	1.51	3.47	2.36	1.39	2.92	1.91

Pluton	Dafangshen			Muniuhe								
Spot no.	DF-8.2	DF-8.3	DF-8.4	MN-3.2	MN-3.3	MN-3.4	MN-3.5	MN-4.1	MN-4.2	MN-4.3	MN-7.1	MN-7.2	MN-7.3
SiO_2	66.58	66.35	68.14	49.37	49.32	51.44	51.69	67.67	65.03	68.85	67.67	65.03	68.85
TiO_2	0.04	0.06	0.03	0.00	0.00	0.00	0.00	0.01	0.02	0.06	0.01	0.02	0.06
Al_2O_3	19.67	20.26	18.56	31.77	32.89	31.17	30.86	18.89	20.66	18.51	18.89	20.66	18.51
Cr_2O_3	0.00	0.00	0.00	0.02	0.00	0.00	0.00	0.04	0.04	0.00	0.04	0.04	0.00
Fe_2O_3	0.00	0.00	0.00	0.00	0.00	0.00	0.00	0.00	0.00	0.00	0.00	0.00	0.00
FeO	0.00	0.00	0.00	0.00	0.00	0.00	0.00	0.00	0.00	0.00	0.00	0.00	0.00

(continued)

Table 7.3 (continued)

Pluton	Dafangshen			Muniuhe									
Spot no.	DF-8.2	DF-8.3	DF-8.4	MN-3.2	MN-3.3	MN-3.4	MN-3.5	MN-4.1	MN-4.2	MN-4.3	MN-7.1	MN-7.2	MN-7.3
MnO	0.02	0.02	0.00	0.00	0.01	0.03	0.02	0.03	0.00	0.02	0.03	0.00	0.02
MgO	0.01	0.00	0.03	0.01	0.01	0.01	0.03	0.00	0.03	0.00	0.00	0.03	0.00
CaO	1.52	2.35	0.31	14.76	15.48	12.85	13.05	0.84	1.27	0.86	0.84	1.27	0.86
Na_2O	11.58	10.63	11.97	4.10	3.56	5.02	4.98	11.73	11.92	12.15	11.73	11.92	12.15
K_2O	0.05	0.07	0.06	0.01	0.04	0.10	0.08	0.18	0.05	0.06	0.18	0.05	0.06
Total	99.47	99.74	99.10	100.04	101.31	100.62	100.71	99.39	99.02	100.51	99.39	99.02	100.51
Si	2.94	2.92	3.01	2.26	2.23	2.33	2.34	2.99	2.90	3.01	2.99	2.90	3.01
Ti	0.00	0.00	0.00	0.00	0.00	0.00	0.00	0.00	0.00	0.00	0.00	0.00	0.00
Al	1.03	1.05	0.97	1.71	1.75	1.66	1.65	0.98	1.08	0.95	0.98	1.08	0.95
Cr	0.00	0.00	0.00	0.00	0.00	0.00	0.00	0.00	0.00	0.00	0.00	0.00	0.00
Fe^{3+}	0.00	0.00	0.00	0.00	0.00	0.00	0.00	0.00	0.00	0.00	0.00	0.00	0.00
Fe^{2+}	0.00	0.00	0.00	0.00	0.00	0.00	0.00	0.00	0.00	0.00	0.00	0.00	0.00
Mn	0.00	0.00	0.00	0.00	0.00	0.00	0.00	0.00	0.00	0.00	0.00	0.00	0.00
Mg	0.00	0.00	0.00	0.00	0.00	0.00	0.00	0.00	0.00	0.00	0.00	0.00	0.00
Ca	0.07	0.11	0.02	0.72	0.75	0.62	0.63	0.04	0.06	0.04	0.04	0.06	0.04
Na	0.99	0.91	1.03	0.36	0.31	0.44	0.44	1.00	1.03	1.03	1.00	1.03	1.03
K	0.00	0.00	0.00	0.00	0.00	0.01	0.01	0.01	0.00	0.00	0.01	0.00	0.00
An	6.74	10.85	1.44	66.48	70.49	58.22	58.85	3.80	5.58	3.73	3.81	5.50	3.74
Ab	92.98	88.76	98.27	33.43	29.32	41.21	40.69	95.26	94.14	95.99	95.24	94.50	96.26
Or	0.28	0.39	0.29	0.09	0.19	0.56	0.47	0.95	0.27	0.28	0.95	0.00	0.00

Note Ion number is calculated based on eight oxygen atoms

Table 7.4 Whole-rock chemical compositions of the gneissic granites in the Jiao-Liao-Ji Belt

Pluton	Dafangshen				Hadabei				Hupiyu		Muniuhe			Simenzi			
Sample	DF-1	DF-2	DF-3	DF-6	HD-2	HD-3	HD-4	HD-7	HP-1	HP-2	MN-1	MN-2	MN-6	SM-1	SM-2	SM-3	SM-5
(wt%)																	
SiO_2	76.7	77.1	76.8	77	73.6	74.1	71.9	70.5	72.4	70.4	72.8	73.8	69.4	72.6	71.5	70.4	71.3
K_2O	5	4.5	5.2	5	3.2	3.3	3.5	3.3	4.9	5	1.8	4.4	3.3	4.6	4.7	3.6	3.1
TiO_2	0.2	0.1	0.1	0.1	0.3	0.3	0.3	0.3	0.3	0.3	0.1	0.3	0.1	0.2	0.3	0.1	0.1
Al_2O_3	10.8	11.2	10.6	11	12.5	11.9	12.4	13.8	12.6	13.1	15.4	12.1	17.1	12.9	13	15	15.2
TFe_2O_3	2.8	2.5	2.1	2	3.7	3.4	5.2	2.1	3.6	4.2	0.6	3.6	1.2	3.4	3.9	1.8	0.8
MgO	0.03	0.01	0.06	0.04	0.06	0.07	0.06	1.41	0.08	0.15	0.27	0.18	0.46	0.12	0.09	0.30	0.32
MnO	0.02	0.02	0.02	0.01	0.01	0.02	0.01	0.04	0.04	0.03	0.01	0.04	0.02	0.04	0.05	0.03	0.02
CaO	0.4	0.5	0.5	0.2	0.69	1.14	0.65	3.16	1.1	1	2.2	1.2	2.5	1.5	1.5	1.6	1.7
Na_2O	2.4	2.8	2.8	3.2	5	4.74	4.8	3.8	3.7	4	5.7	3	4.7	3.7	3.7	5.7	6.2
P_2O_5	b.d.	b.d.	0.08	b.d.	b.d.	0.008	0.007	0.011	0.074	0.01	0.07	0.014	0.02	0.016	0.017	0.01	0.04
LOl	0.6	0.2	0.6	0.4	0	0	0.2	0.5	0.2	0.8	0.3	0.3	0.3	-0.1	0.3	0.3	0.3
Total	98.9	98.9	98.9	99	99	99	99	99	99	99	99	98.9	99	99	99	99	99
A/NK	1.2	1.2	1.0	1.0	1.1	1.0	1.1	1.4	1.1	1.1	1.4	1.2	1.5	1.2	1.2	1.1	1.1
A/CNK	1.1	1.1	0.9	1.0	1.0	0.9	1.0	0.9	0.9	0.9	1.0	1.0	1.1	0.9	0.9	0.9	0.9
K_2O/Na_2O	2.1	1.6	1.9	1.6	0.6	0.7	0.7	0.9	1.3	1.3	0.3	1.5	0.7	1.2	1.3	0.6	0.5
Mg#	4.2	1.7	11.7	8.2	7.1	8.4	5.1	74.9	8.9	13.7	66.7	18.2	63.2	13.6	9.1	42.5	64.2
(ppm)																	
Sc	1.7	1.5	1.6	1	3.2	3.7	4	5.6	4.2	5.7	1	4.8	2.6	3.4	5.8	0.9	0.8
Ti	1011	761	839	822	1672	1980	1967	1961	1887	2354	401	1964	607	1387	2388	474	475
V	1.8	1.7	1.7	1.3	7	5	7	40.8	2.8	3.7	4.7	6.8	10.6	3.2	2.7	2	3.7
Cr	1	0.5	1.6	1.1	4	1.2	1.8	46	4.7	2.1	2.6	4.7	3.6	3	2.1	3.1	2.4
Mn	207	176	133	64	97.3	141.4	122.7	310.6	350.2	233	83.9	350.6	164	370.8	443.6	250	200
Co	0.2	0.1	0.3	0.2	1.4	0.9	3.3	4.8	0.5	0.7	0.8	1.4	1.8	0.7	1.3	0.4	0.8
Ni	0.8	0.4	1	0.9	2.4	3.9	2.3	11.9	3	1.9	2	2.9	1.3	0.8	1.4	2.6	2.3
Cu	1	0.4	0.8	1	1.9	3.4	5.7	0.9	3.4	4.1	1.4	2.3	6.8	1.5	4.4	0.9	1.3
Zn	34.3	27.1	40.3	22	25.6	22.7	42.7	59.6	29.9	60.5	29.3	60.7	42.5	32.6	45.6	46.3	58.5
Ga	21.9	21.2	20.9	24	19.5	21.4	22	18.6	21	24.1	15.3	21.8	19.7	21.3	24	16.8	15.6
Rb	247	191	237	200	81.9	99.2	92.5	87.9	136	161	56.2	180.4	173	131.1	146.9	86.5	79.5
Sr	22	28.7	29.8	16	89.6	116.5	102.7	609.8	52.3	55.5	880	136.5	389	167.6	190.1	280	570
Y	46.6	74.2	48.3	60	38	50.9	38.7	8.1	57.2	47.2	3	35.3	5.5	34.3	76.7	9	8.6
Zr	349	323	364	326	379.2	439.8	409.4	148.5	374	460	63.9	391.6	29.4	278.4	569.3	57.9	73.8
Nb	27.1	16.6	20.5	37	21.2	27.9	19.1	9.9	24.7	35.1	2	23.6	8.3	17.7	33.7	5	3.6

(continued)

Table 7.4 (continued)

Pluton	Dafangshen				Hadabei				Hupiyu		Muniuhe			Simenzi			
Sample	DF-1	DF-2	DF-3	DF-6	HD-2	HD-3	HD-4	HD-7	HP-1	HP-2	MN-1	MN-2	MN-6	SM-1	SM-2	SM-3	SM-5
Cs	1.6	0.8	1.7	0.6	0.5	0.4	0.4	0.8	1.6	3.9	1.1	2.5	5.5	0.4	0.4	0.1	0.2
Ba	188	167	203	122	1057	1194	1032	1282	821.8	779	970	1114	1911	1099	1344	965	1169
La	66	123	160	74	24.1	49.1	32.7	26.7	11.2	7.3	4.9	54.3	1.8	14.3	106	2.8	4.2
Ce	195	253	256	155	66.7	109.3	85.1	50.5	31.9	21	9.6	115.2	3.4	40.2	185.4	7.4	6.2
Pr	16.8	31.9	35.9	19	9.2	13.3	11.4	5.4	5.5	3.9	1.2	13.7	0.4	5.9	20.3	1.1	1
Nd	58.1	114	124	65	35.8	49.3	43	17.8	26.3	20	4.2	48.9	1.7	24.1	72.2	4.4	3.8
Sm	11.4	23.9	24.7	13	7.5	10.1	8.6	2.8	8.2	6.8	0.8	9.3	0.5	5.8	14.9	1.1	0.9
Eu	0.3	0.7	0.7	0.4	1.6	1.9	1.6	1	1.4	1.3	0.5	1.6	0.6	1.2	2.4	0.6	0.5
Gd	10.2	22.4	21.4	12	7.3	9.9	7.9	2.3	9.2	7.7	0.7	8.6	0.7	6	14.6	1.2	1
Tb	1.6	3.3	2.7	1.9	1.1	1.5	1.2	0.3	1.6	1.3	0.1	1.2	0.1	1	2.2	0.2	0.2
Dy	10.2	19	13.2	12	7.2	9.6	7.1	1.6	10.3	8.4	0.5	7.2	0.8	6.3	13.9	1.3	1.1
Ho	2.1	3.4	2.1	2.5	1.5	2	1.5	0.3	2.2	1.7	0.1	1.4	0.2	1.3	2.9	0.3	0.3
Er	6.2	8.2	4.6	7.3	4.3	5.7	4.3	0.9	6.5	5	0.3	3.8	0.6	3.9	8.4	0.9	0.9
Tm	0.9	0.9	0.5	1	0.6	0.8	0.6	0.1	0.9	0.7	0	0.5	0.1	0.6	1.2	0.1	0.1
Yb	5.3	5	2.7	6.6	4.1	5	4.1	0.9	6.2	4.9	0.3	3.1	0.7	3.8	8	1.1	1
Lu	0.7	0.6	0.4	0.9	0.6	0.7	0.6	0.1	0.9	0.7	0	0.4	0.1	0.6	1.1	0.2	0.2
Hf	10.8	10.6	10.8	11	9.5	10.5	9.8	3.9	8.8	11.5	1.8	9.9	1	6.7	13.2	1.7	1.9
Ta	1.5	1.1	1.3	2	1.4	1.7	1.4	0.6	1.4	2.1	0.1	1.4	0.8	1	2.5	0.3	0.3
Pb	13.9	14.8	17.1	10	7.8	8	9.1	11.3	6.1	7.4	18	9.9	38.7	4.9	9.3	4	7.3
Th	37.6	49	48.4	33	6.7	12.7	4.9	7.2	20.5	13.5	1.3	21	0.9	5.3	25.1	0.5	0.4
U	2.6	4.3	2.9	3.1	1.8	1.7	2.7	2.4	2.7	3	0.4	4.3	2.5	1.6	2.8	0.7	0.7
Sr/Y	0.5	0.4	0.6	0.3	2.4	2.3	2.7	75.3	0.9	1.2	293.5	3.9	70.7	4.9	2.5	31.1	66.3
ΣREE	385	609	649	371	171.7	268.2	209.6	110.8	122.2	90.8	23.1	269.2	11.6	115	453.6	22.7	21.3
La_N/Yb_N	8.9	17.6	41.9	8	4.2	7	5.7	22.1	1.3	1.1	11.7	12.4	2	2.7	9.5	1.9	2.9
Eu/Eu*	0.1	0.1	0.1	0.1	0.7	0.6	0.6	1.1	0.5	0.5	1.9	0.5	3.3	0.6	0.5	1.5	1.7
K/Ta	####	####	####	###	18187	15446	19892	43763	27849	####	####	25008	####	36602	14959	####	####
Ba/La	2.8	1.4	1.3	1.6	43.9	24.3	31.6	48.0	73.4	####	198.0	20.5	####	76.9	12.7	344.7	278.2
Zr/Hf	32.3	30.5	33.7	30.4	39.9	41.9	41.8	38.1	42.5	40.0	35.5	39.6	29.4	41.6	43.1	34.1	38.8
$TE_{1,3}$	0.12	0.21	0.19	0.12	0.07	0.09	0.07	0.03	0.06	0.04	0.01	0.08	0.00	0.05	0.14	0.01	0.01
T_{Zr} (°C)	870	870	870	870	870.3	870.3	870.3	870.3	870.3	870	870	870.3	870	870.3	870.3	870	870

Note $Eu/Eu^* = Eu_N/((Sm_N + Gd_N)/2)$

T_{Zr} (°C)—zircon saturation temperature, calculated using the geothermometer of Watson and Harrison (1983)

$TE_1 = (((Ce/Ce^* \times Pr/Pr^*)^{0.5} \times (Tb/Tb^* \times Dy/Dy^*)^{0.5})^{0.5}$,—the degree of the tetrad effect (Irber 1999)

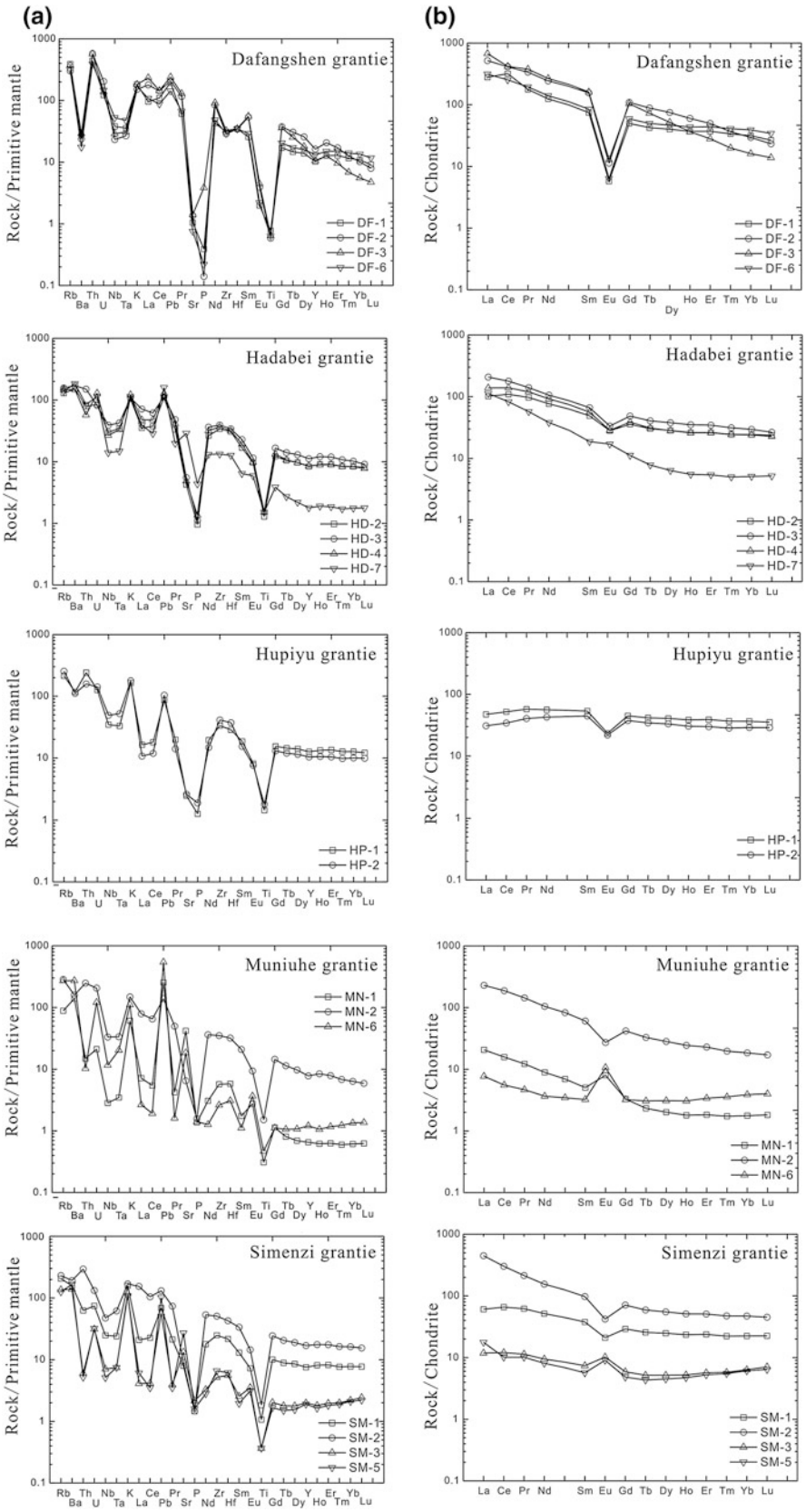

Fig. 7.7 **a** Chondrite-normalized REE patterns of ths gneissic granites. Normalization values of chondrite are from Sun and McDonough (1989). **b** Primitive mantle (PM)-normalized spidergrams of the granites. PM values are from Sun and McDonough (1989). *DF* Dafangshen; *HD* Hadabei; *HP* Hupiyu; *MN* Muniuhe; *SM* Simenzi

suggest that they are originally mantle-derived mafic magma and then modified by mixing/mingling with surrounding felsic melts (Holden et al. 1987; Vernon et al. 1988; Bonin 2004; Sklyarov and Fedorovsky 2006; Chen et al. 2008, 2009; Feeley et al. 2008; Ma et al. 2013) for evidence as below. (1) MMEs are elongated in shape without solid-stated deformation (Fig. 7.3b), due to stretching plastically within a partially crystallized, convective magma (Chen et al. 2008, 2009). (2) There are some plagioclase inclusions in the hornblende crystal from the MME (Fig. 7.3d), indicating that the mafic magma injected into the felsic magma and captured the plagioclase crystallized in the early period. (3) MMEs show more fine-grained and equigranular textures than host rocks (Fig. 7.3c) and many needle-like apatites can be seen in the MMEs (Fig. 7.3c), suggesting that the hot mafic magma has undergone a quenching process when injected into the felsic magma with lower temperatures. The existence of MMEs is typical of a mingling/mixing process for the genesis of the host magma (Clynne 1999; Kemp 2004; Chen et al. 2009).

Second, some plagioclases near the MMEs in the host rock show complicated compositional and textural disequilibrium (Fig. 7.3e, f), which commonly results from magma mixing between intermediate-mafic and felsic melts (Anderson 1976; Janoušek et al. 2004; Chen et al. 2009). As shown in Fig. 7.3h, the Na-rich plagioclase core (An_{18}) was crystallized from felsic magma, and the relatively Ca-rich overgrowths (An_{35} and An_{39}) may result from two pulses of input of mafic magma into the magma system and subsequent magma mixing (Chen et al. 2013).

Third, the whole-rock Nd isotopic compositions vary significantly ($\varepsilon_{Nd}(t) = -8.6$ to 1.5; Fig. 7.8), even for samples from a single pluton. This argues against a process of closed system magma evolution (Griffin et al. 2002; Kemp and Hawkesworth 2006), rather, a magma mixing process between two end members with distinct Nd isotopic compositions is required. This is consistent with the large variation of $\varepsilon_{Hf}(t)$ values (from −1.27 to 5.58; Fig. 7.9) of zircons from each pluton. Large Hf isotopic variation is also considered as having been resulted from a mixing/mingling process between magmas with distinct sources by some other researchers (Kemp and Hawkesworth 2006; Yang et al. 2008; Zhang et al. 2011) (Tables 7.5 and 7.6).

7.6 Source Characteristics

Potential end members that may have contributed to the formation of these granites are felsic magma derived from partial melting of the basement and mafic magma from the mantle. The gneissic granites have a wide range of whole-rock $\varepsilon_{Nd}(t)$ values (−8.6 to 1.5). The very negative $\varepsilon_{Nd}(t)$ values of some samples (as low as −8) suggest that the felsic end member should have been originated from partial melting of Archean basement rocks. This is supported by the ages of the inherited zircons from these gneissic granites mentioned above (2.53–2.78 Ga), and is compatible with the protolith ages (2.5–2.6 Ga) obtained by Kröner et al. (1988) and Zhao et al. (2001) for the basement rocks beneath the East Block. The Archean basement of the North China Craton is composed mainly of intermediate-mafic granulite/amphibolite and TTG gneisses (Jahn and Ernst 1990; Liu et al. 1992; Zhao et al. 2005). The Dafangshen, Hupiyu and Simenzi granites are rich in potassium, with

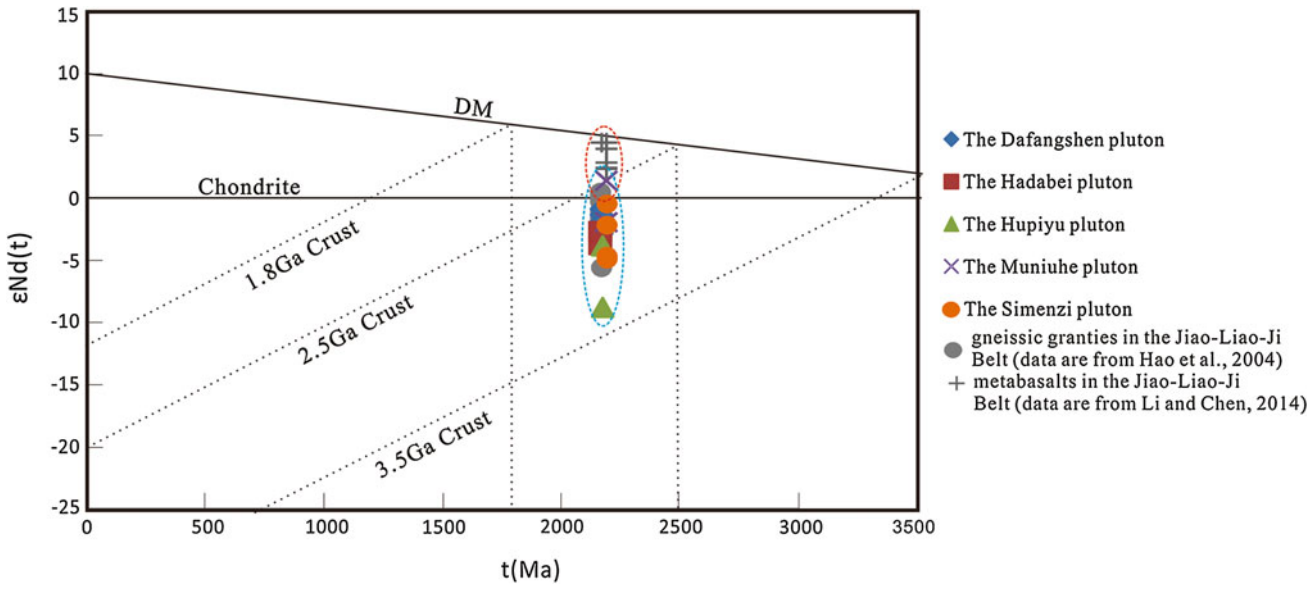

Fig. 7.8 Whole-rock Nd isotopic data of the gneissic granites

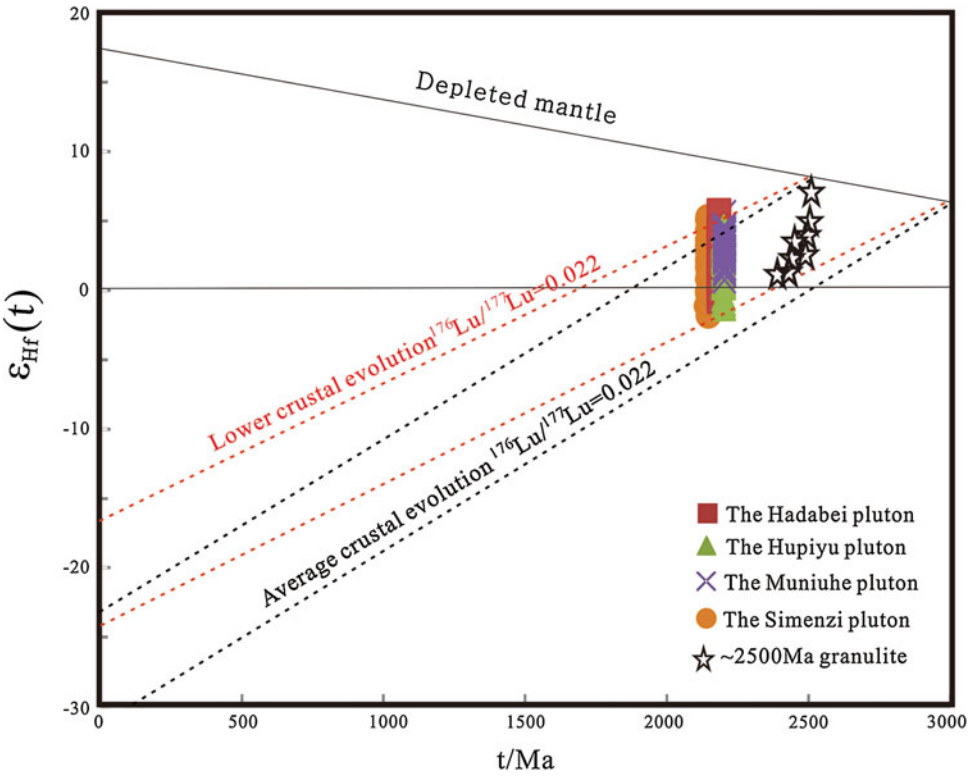

Fig. 7.9 Zircon Hf isotopic compositions of the granites. Zircon $\varepsilon_{Hf}(t)$ values were calculated at the crystallization ages of these granites. Values of ~2500 Ma granulite are from Jiang et al. (2013)

Table 7.5 In-situ Hf isotopic data for zircons of the gneissic granites

Spot	$^{176}Yb/^{177}Hf$	$^{176}Lu/^{177}Hf$	$^{176}Hf/^{177}Hf$	2σ	Age	$\varepsilon_{Hf}(t)$	$f_{Lu/Hf}$	T_{DM1}(Hf)(Ma)	T_{DM2}(Hf)(Ma)
Hadabei									
HD-2-1	0.081416	0.001535	0.281519	0.000024	2173	2.1	−0.95	2467	2636
HD-2-2	0.077523	0.001437	0.281426	0.000028	2173	−1.1	−0.96	2590	2831
HD-2-3	0.090094	0.001663	0.281543	0.000026	2173	2.7	−0.95	2442	2595
HD-2-4	0.065516	0.001235	0.281535	0.000028	2173	3.1	−0.96	2425	2574
HD-2-5	0.072699	0.001355	0.281602	0.000027	2173	5.3	−0.96	2340	2437
HD-2-6	0.100365	0.002538	0.281534	0.000023	2173	1.1	−0.92	2513	2694
HD-2-7	0.071790	0.001327	0.281517	0.000025	2173	2.3	−0.96	2456	2622
HD-2-8	0.087769	0.001598	0.281482	0.000028	2173	0.7	−0.95	2523	2723
HD-2-9	0.082085	0.001457	0.281488	0.000026	2173	1.1	−0.96	2505	2697
HD-2-10	0.046407	0.000861	0.281402	0.000029	2173	−1.1	−0.97	2584	2832
HD-2-11	0.047838	0.000954	0.281466	0.000024	2173	1.0	−0.97	2502	2700
HD-2-12	0.066753	0.001304	0.281563	0.000025	2173	4.0	−0.96	2391	2519
HD-2-13	0.057992	0.001174	0.281491	0.000023	2173	1.6	−0.96	2482	2665
HD-2-14	0.068398	0.001366	0.281439	0.000022	2173	−0.5	−0.96	2567	2796
HD-2-15	0.092179	0.001819	0.281481	0.000025	2173	0.3	−0.95	2539	2745
HD-2-16	0.061374	0.001243	0.281488	0.000023	2173	1.4	−0.96	2491	2678
HD-2-17	0.093567	0.001855	0.281514	0.000024	2173	1.4	−0.94	2495	2676
HD-2-18	0.073175	0.001458	0.281475	0.000025	2173	0.6	−0.96	2523	2726
HD-2-19	0.051215	0.000997	0.281452	0.000025	2173	0.5	−0.97	2524	2734
HD-2-20	0.044025	0.000835	0.281434	0.000026	2173	0.1	−0.97	2538	2759
HD-2-21	0.055230	0.001028	0.281477	0.000030	2173	1.3	−0.97	2492	2682

(continued)

Table 7.5 (continued)

Spot	$^{176}Yb/^{177}Hf$	$^{176}Lu/^{177}Hf$	$^{176}Hf/^{177}Hf$	2σ	Age	$\varepsilon_{Hf}(t)$	$f_{Lu/Hf}$	T_{DM1}(Hf)(Ma)	T_{DM2}(Hf)(Ma)
HD-2-22	0.057294	0.001066	0.281465	0.000026	2173	0.8	−0.97	2511	2712
HD-2-23	0.084556	0.001544	0.281545	0.000027	2173	3.0	−0.95	2431	2580
HD-2-24	0.063984	0.001187	0.281489	0.000022	2173	1.5	−0.96	2486	2671
HD-2-25	0.071754	0.001606	0.281599	0.000024	2173	4.8	−0.95	2360	2467
HD-2-26	0.068927	0.001250	0.281434	0.000026	2173	−0.5	−0.96	2566	2797
HD-2-27	0.106870	0.001855	0.281486	0.000029	2173	0.4	−0.94	2534	2737
HD-2-28	0.070238	0.001215	0.281412	0.000024	2173	−1.3	−0.96	2594	2842
HD-2-29	0.099390	0.002123	0.281563	0.000025	2173	2.8	−0.94	2444	2593
HD-2-30	0.074455	0.001353	0.281508	0.000025	2173	1.9	−0.96	2470	2644
Hupiyu									
HP-1-1	0.074395	0.001386	0.281494	0.000021	2183.7	1.6	−0.96	2492	2671
HP-1-2	0.044793	0.000846	0.281464	0.000023	2183.7	1.4	−0.97	2498	2688
HP-1-3	0.050848	0.000967	0.281506	0.000026	2183.7	2.7	−0.97	2448	2607
HP-1-4	0.088921	0.001619	0.281475	0.000028	2183.7	0.6	−0.95	2534	2734
HP-1-5	0.053146	0.001007	0.281548	0.000026	2183.7	4.1	−0.97	2393	2518
HP-1-6	0.075915	0.001421	0.281539	0.000029	2183.7	3.2	−0.96	2432	2576
HP-1-7	0.071330	0.001294	0.281483	0.000025	2183.7	1.4	−0.96	2501	2687
HP-1-8	0.057529	0.001036	0.281498	0.000027	2183.7	2.3	−0.97	2464	2631
HP-1-9	0.074812	0.001346	0.281468	0.000026	2183.7	0.8	−0.96	2525	2725
HP-1-10	0.088741	0.001577	0.281476	0.00003	2183.7	0.7	−0.95	2530	2728
HP-1-11	0.099652	0.001774	0.281559	0.00003	2183.7	3.4	−0.95	2427	2564
HP-1-12	0.085097	0.001539	0.281535	0.00003	2183.7	2.9	−0.95	2445	2595
HP-1-13	0.069756	0.001278	0.281489	0.000027	2183.7	1.6	−0.96	2492	2672
HP-1-14	0.094813	0.001765	0.281519	0.00003	2183.7	2.0	−0.95	2482	2651
HP-1-15	0.035352	0.000687	0.281448	0.000025	2183.7	1.0	−0.98	2509	2709
HP-1-16	0.075686	0.001474	0.281545	0.000025	2183.7	3.3	−0.96	2427	2567
HP-1-17	0.089821	0.001733	0.28162	0.000026	2183.7	5.6	−0.95	2338	2426
HP-1-18	0.066379	0.001308	0.281495	0.000029	2183.7	1.8	−0.96	2485	2662
HP-1-19	0.071755	0.001419	0.281454	0.000029	2183.7	0.2	−0.96	2550	2762
HP-1-20	0.07638	0.001479	0.281483	0.000031	2183.7	1.1	−0.96	2513	2704
HP-1-21	0.046277	0.000901	0.281462	0.000026	2183.7	1.2	−0.97	2504	2697
HP-1-22	0.073131	0.001373	0.281446	0.000026	2183.7	−0.1	−0.96	2558	2775
HP-1-23	0.077632	0.001406	0.281431	0.000031	2183.7	−0.6	−0.96	2581	2811
HP-1-24	0.123147	0.002167	0.281567	0.000027	2183.7	3.1	−0.93	2441	2582
HP-1-25	0.067404	0.001282	0.28145	0.000028	2183.7	0.2	−0.96	2546	2758
HP-1-26	0.082199	0.001428	0.28145	0.000028	2183.7	0.0	−0.96	2556	2772
HP-1-27	0.09599	0.00169	0.281586	0.000024	2183.7	4.4	−0.95	2383	2497
HP-1-28	0.099401	0.001691	0.281481	0.000028	2183.7	0.7	−0.95	2530	2728
HP-1-29	0.067734	0.001195	0.281498	0.000022	2183.7	2.1	−0.96	2474	2645
HP-1-30	0.044159	0.000818	0.281477	0.000023	2183.7	1.9	−0.98	2478	2657
Muniuhe									
MN-6-1	0.068236	0.001302	0.281523	0.000019	2200.6	3.2	−0.96	2446	2590
MN-6-2	0.064231	0.001825	0.281468	0.000019	2200.6	0.4	−0.95	2558	2759
MN-6-3	0.064976	0.001227	0.281555	0.000029	2200.6	4.4	−0.96	2397	2513
MN-6-4	0.089113	0.001725	0.281519	0.000022	2200.6	2.4	−0.95	2479	2638

(continued)

Table 7.5 (continued)

Spot	$^{176}Yb/^{177}Hf$	$^{176}Lu/^{177}Hf$	$^{176}Hf/^{177}Hf$	2σ	Age	$\varepsilon_{Hf}(t)$	$f_{Lu/Hf}$	T_{DM1}(Hf)(Ma)	T_{DM2}(Hf)(Ma)
MN-6-6	0.036055	0.000868	0.28151	0.000019	2200.6	3.3	−0.97	2436	2579
MN-6-7	0.075335	0.001412	0.281455	0.000021	2200.6	0.6	−0.96	2548	2749
MN-6-8	0.089766	0.001845	0.281424	0.000021	2200.6	−1.2	−0.94	2621	2857
MN-6-9	0.07596	0.001384	0.281494	0.00002	2200.6	2.0	−0.96	2492	2661
MN-6-10	0.096975	0.001864	0.281491	0.00002	2200.6	1.2	−0.94	2528	2712
MN-6-12	0.069868	0.001299	0.281537	0.00003	2200.6	3.7	−0.96	2427	2559
MN-6-13	0.05172	0.000965	0.28149	0.000029	2200.6	2.5	−0.97	2470	2632
MN-6-14	0.056778	0.001194	0.281416	0.000028	2200.6	−0.5	−0.96	2587	2815
MN-6-15	0.066777	0.001233	0.281468	0.000029	2200.6	1.3	−0.96	2518	2704
MN-6-16	0.096858	0.001738	0.281519	0.000026	2200.6	2.4	−0.95	2480	2639
MN-6-17	0.04692	0.00087	0.281488	0.000022	2200.6	2.6	−0.97	2467	2627
MN-6-18	0.088128	0.001722	0.281559	0.000025	2200.6	3.8	−0.95	2423	2550
MN-6-19	0.096699	0.001725	0.28152	0.000026	2200.6	2.4	−0.95	2478	2636
MN-6-20	0.079048	0.001882	0.281582	0.000025	2200.6	4.4	−0.94	2401	2514
MN-6-21	0.039258	0.000737	0.281491	0.000026	2200.6	2.9	−0.98	2454	2609
MN-6-22	0.052304	0.001005	0.281522	0.000022	2200.6	3.6	−0.97	2429	2565
MN-6-23	0.060564	0.001121	0.28146	0.000027	2200.6	1.2	−0.97	2521	2712
MN-6-24	0.046786	0.001007	0.281397	0.000024	2200.6	−0.9	−0.97	2600	2839
MN-6-25	0.071917	0.001364	0.281481	0.000022	2200.6	1.6	−0.96	2509	2688
MN-6-26	0.098614	0.001963	0.281494	0.000019	2200.6	1.1	−0.94	2531	2714
MN-6-27	0.037522	0.000763	0.281455	0.000021	2200.6	1.5	−0.98	2505	2690
MN-6-28	0.074898	0.001485	0.281502	0.000025	2200.6	2.1	−0.96	2487	2653
MN-6-30	0.079432	0.001923	0.281469	0.000025	2200.6	0.3	−0.94	2563	2765
Simenzi									
SM-1-1	0.118087	0.001896	0.281571	0.000023	2203	4.0	−0.94	2418	2538
SM-1-2	0.082921	0.001361	0.281538	0.000018	2203	3.7	−0.96	2429	2561
SM-1-3	0.097105	0.001612	0.281547	0.000019	2203	3.6	−0.95	2433	2565
SM-1-4	0.123158	0.002059	0.281585	0.000023	2203	4.3	−0.94	2408	2522
SM-1-5	0.089992	0.001561	0.281544	0.000023	2203	3.6	−0.95	2434	2566
SM-1-6	0.146659	0.002533	0.281567	0.000022	2203	2.9	−0.92	2465	2605
SM-1-7	0.105565	0.001815	0.28155	0.00002	2203	3.4	−0.95	2442	2577
SM-1-8	0.075895	0.00138	0.281555	0.000021	2203	4.2	−0.96	2407	2526
SM-1-9	0.123441	0.002152	0.281624	0.00002	2203	5.5	−0.94	2359	2445
SM-1-10	0.078022	0.001429	0.281517	0.00002	2203	2.8	−0.96	2463	2614
SM-1-11	0.101877	0.001895	0.281563	0.00002	2203	3.7	−0.94	2429	2555
SM-1-12	0.139913	0.002588	0.281551	0.000019	2203	2.3	−0.92	2492	2645
SM-1-13	0.071504	0.00133	0.281563	0.000018	2203	4.6	−0.96	2393	2503
SM-1-14	0.085331	0.001575	0.281519	0.000024	2203	2.7	−0.95	2470	2623
SM-1-15	0.062735	0.001184	0.281512	0.000022	2203	3.0	−0.96	2454	2602
SM-1-16	0.05278	0.000967	0.281477	0.000021	2203	2.1	−0.97	2488	2659
SM-1-17	0.045639	0.000869	0.281436	0.000022	2203	0.8	−0.97	2538	2740
SM-1-18	0.118256	0.00207	0.28158	0.000024	2203	4.1	−0.94	2416	2534
SM-1-19	0.037631	0.000678	0.281455	0.000019	2203	1.7	−0.98	2499	2681
SM-1-20	0.11944	0.002047	0.28156	0.000023	2203	3.4	−0.94	2443	2576
SM-1-21	0.093779	0.00156	0.281489	0.000018	2203	1.6	−0.95	2510	2687

(continued)

Table 7.5 (continued)

Spot	$^{176}Yb/^{177}Hf$	$^{176}Lu/^{177}Hf$	$^{176}Hf/^{177}Hf$	2σ	Age	$\varepsilon_{Hf}(t)$	$f_{Lu/Hf}$	T_{DM1}(Hf)(Ma)	T_{DM2}(Hf)(Ma)
SM-1-22	0.116543	0.001937	0.281526	0.000023	2203	2.4	−0.94	2484	2640
SM-1-23	0.094341	0.001611	0.281539	0.000025	2203	3.3	−0.95	2444	2582
SM-1-24	0.105058	0.001704	0.281536	0.000017	2203	3.1	−0.95	2454	2597
SM-1-25	0.143297	0.002384	0.281599	0.000021	2203	4.3	−0.93	2410	2521
SM-1-26	0.099439	0.001666	0.281562	0.00002	2203	4.1	−0.95	2415	2537
SM-1-27	0.106738	0.001827	0.281494	0.000023	2203	1.4	−0.94	2521	2701
SM-1-28	0.035731	0.000676	0.281441	0.00002	2203	1.2	−0.98	2518	2711
SM-1-29	0.064531	0.001129	0.281551	0.000019	2203	4.5	−0.97	2397	2511
SM-1-30	0.097948	0.001748	0.281581	0.000024	2203	4.6	−0.95	2394	2502

Note $\varepsilon_{Hf}(0) = (((^{176}Hf/^{177}Hf)_S/(^{176}Hf/^{177}Hf)_{CHUR,0} - 1) \times 10{,}000$, $f_{Lu/Hf} = (^{176}Lu/^{177}Hf)_S/(^{176}Lu/^{177}Hf)_{CHUR} - 1$
$\varepsilon_{Hf}(t) = (((^{176}Hf/^{177}Hf)_S - (^{176}Lu/^{177}Hf)_S \times (e^{\lambda t} - 1))/((^{176}Hf/^{177}Hf)_{CHUR,0} - (^{176}Lu/^{177}Hf)_{CHUR} \times (e^{\lambda t} - 1)) - 1) \times 10{,}000$
$T_{DM1}(Hf) = 1/l \times (1 + ((^{176}Hf/^{177}Hf)_S - (^{176}Hf/^{177}Hf)_{DM})/((^{176}Lu/^{177}Hf)_S - (^{176}Lu/^{177}Hf)_{DM}))$
$T_{DM2}(Hf) = T_{DM1}(Hf) - (T_{DM1}(Hf) - t)((f_{CC} - f_S)/(f_{CC} - f_{DM}))$
where, $(^{176}Lu/^{177}Hf)_S$ and $(^{176}Hf/^{177}Hf)_S$ are the measured values of samples; $(^{176}Lu/^{177}Hf)_{CHUR} = 0.0332$ and $(^{176}Hf/^{177}Hf)_{CHUR,0} = 0.282772$; $(^{176}Lu/^{177}Hf)_{DM} = 0.0384$ and (176Hf/177Hf)DM = 0.28325; $f_{CC} = -0.548$ (average continental crust), $f_{DM} = 0.16$, t = crystallization time of zircon, $\lambda = 1.865 \times 10^{-11}$ $year^{-1}$ (Soderlund et al. 2004) are used in calculation

Table 7.6 Sm–Nd isotopic data of gneissic granites in the Jiao-Liao-Ji Belt

Sample	Sm (ppm)	Nd (ppm)	$^{147}Sm/^{144}Nd$	$^{143}Nd/^{144}Nd$	2σ	T (Ma)	I_{Nd}	$\varepsilon_{Nd}(0)$	$\varepsilon_{Nd}(T)$	$f_{Sm/Nd}$	T_{DM1}	T_{DM2}
Dafangshen												
DF-1	11.386	58.06	0.124421129	0.511536	2	2180	0.509749397	−21.497	−1.258	−0.3675	2740	2702
DF-2	23.86	113.74	0.13309361	0.51158452	3	2180	0.509673386	−20.55	−2.749	−0.3234	2941	2821
DF-3	24.66	124.24	0.125930701	0.51158202	5	2180	0.509773741	−20.599	−0.78	−0.3598	2708	2664
DF-6	12.943	65.25	0.125850349	0.51153065	1	2180	0.509723525	−21.601	−1.765	−0.3602	2793	2743
Hadabei												
HD-2	7.482	35.76	0.132745615	0.51158772	3	2173	0.509687748	−20.488	−2.646	−0.3251	2923	2807
HD-3	10.138	49.26	0.130574349	0.51150663	3	2173	0.509637735	−22.07	−3.627	−0.3362	2993	2886
HD-4	8.568	43	0.126418605	0.5115008	2	2173	0.509691385	−22.183	−2.575	−0.3573	2862	2802
Hupiyu												
HP-1	8.208	26.3	0.198007477	0.51221656	2	2184	0.509368053	−8.221	−8.636	0.00665	8835	3269
HP-2	6.828	19.962	0.217014849	0.51273939	3	2184	0.509617446	1.9778	−3.744	0.10328	####	2985
Muniuhe												
MN-1	0.771	4.156	0.117700641	0.51139916	22	2200	0.509693442	−24.166	−1.844	−0.4016	2764	2765
MN-6	0.495	1.712	0.18344312	0.51252019	4	2200	0.509861731	−2.2981	1.4576	−0.0674	3150	2500
Simenzi												
SM-1	5.766	24.14	0.151543517	0.51174952	5	2203	0.509550334	−17.332	−4.574	−0.2296	3407	2985
SM-2	14.874	72.197	0.13070994	0.5116597	3	2203	0.509762849	−19.084	−0.405	−0.3355	2721	2653
SM-3	1.13	4.414	0.162422468	0.51189613	29	2203	0.50953907	−14.472	−4.795	−0.1743	3694	3001
SM-5	0.864	3.78	0.145018007	0.51178192	4	2203	0.509677432	−16.7	−2.081	−0.2627	3016	2786

Note $\varepsilon_{Nd} = (((^{143}Nd/^{144}Nd)_S/(^{143}Nd/^{144}Nd)_{CHUR} - 1) \times 10{,}000$, $f_{Sm/Nd} = (^{147}Sm/^{144}Nd)_S/(^{147}Sm/^{144}Nd)_{CHUR} - 1$, $T_{DM1} = 1/\lambda \times \ln(1 + ((^{143}Nd/^{144}Nd)_S - (^{143}Nd/^{144}Nd)_{DM})/((^{147}Sm/^{144}Nd)_S - (^{147}Sm/^{144}Nd)_{DM}))$, $T_{DM2} = T_{DM1} - (T_{DM1} - t)((-0.4 - f_{Sm/Nd})(-0.4 - 0.08592))$, $^{143}Nd/^{144}Nd_{CHUR} = 0.512638$, $^{147}Sm/^{144}Nd_{CHUR} = 0.1967$, $^{143}Nd/^{144}Nd_{DM} = 0.51315$, $^{147}Sm/^{144}Nd_{DM} = 0.2137$; $\lambda_{Rb} = 1.42 \times 10^{-11}$/year, and $\lambda_{Sm} = 6.54 \times 10^{-12}$/year

K_2O/Na_2O ratios in the ranges of 1.6–2.1, 1.3 and 0.5–1.3, respectively. They also have relatively low $\varepsilon_{Nd}(t)$ values (−2.8 to −0.8, −8.6 to −3.7, −4.8 to −0.41, respectively), which are lower than that of the late Archean mafic-ultra mafic amphibolites at 2.2 Ga (−1.19 to 10.51), but in the range of TTG's ε_{Nd} (2.2 Ga) (−16.41 to 1.94). Hence, we suggest that the source of the felsic end member of the Dafangshen, Hupiyu and Simenzi plutons is dominated by the Archean TTG gneisses, which is consistent with the high contents of SiO_2 (70.4–77.1 wt%) of the these plutons. The Muniuhe and Hadabei plutons, however, show relatively low K_2O/Na_2O ratios (mostly <1) and high $\varepsilon_{Nd}(t)$ values (−3.6 to 1.46), suggesting that some amounts of the late Archean amphibolites could have been involved in the source of the felsic end member of the two granite plutons.

We suggest that the other end member having contributed to forming the gneissic granites is mafic magma derived from a mantle source that was previously metasomatized by subduction zone fluids/melts released from a down-going oceanic slab. This is first supported by the positive $\varepsilon_{Nd}(t)$ values (+1.5 for sample MN-6) and zircon $\varepsilon_{Hf}(t)$ values (+5.6 for sample HP-1) of some gneissic granite samples, which is indicative of involvement of mantle-derived magma in the source. The abundance of euhedral hornblende in MMEs (Fig. 7.3c) and in coeval meta-mafic rocks (Li et al. 2003) suggests that the parental magma of the MMEs should be a hydrous basaltic magma (Chen et al. 2009, 2013), possibly derived from a mantle source above a subduction zone. The coeval meta-mafic rocks show high LILEs, such as Sr, Ba, Th and depletion of HSFEs, such as Nb, Ta, and Ti, which, along with the typical calc-alkaline features of the basaltic rocks (Faure et al. 2004; Wang et al. 2012; Li and Chen 2014), suggest a metasomatized lithospheric mantle for the source of the basalts. In addition, the meta-mafic rocks have extremely high K/Ta (>20,000, data from Li and Chen 2014) and Ba/La ratios (1.3–1062). This is probably caused by the high mobility of K and Ba in subduction zone fluids (Huang et al. 2001).

7.7 Geodynamic Setting

Most researchers believe that the Paleoproterozoic Liaoji Belt was formed in an intra-continental rifting setting on the NCC (Zhang and Yang 1988; Peng and Palmer 1995; Chen et al. 2003; Li et al. 2003, 2005; Luo et al. 2004, 2008; Zhao et al. 2005; Li and Zhao 2007). Some others, however, suggested that the Paleoproterozoic Belt formed as a result of arc-continent collision at ca. 1.9 Ga (Bai 1993; He and Ye 1998a, b; Faure et al. 2004; Lu et al. 2006; Wang et al. 2011; Meng et al. 2013). Our new data on the Paleoproterozoic gneissic granites suggest a continental arc setting for these granites and thus for the Paleoproterozoic belt, and the arguments are as below.

Most gneissic granites in the Paleoproterozoic belt show calc-alkaline affinity, although some of them show features of A-types, e.g., the Dafangshen pluton, due probably to addition of boron in magma system. The calc-alkaline affinity is manifested by both the chemical compositions of I-type and the common occurrence of hornblende, apatite, magnetite and sphene, typical features of arc magmas. In addition, the arc affinity of the gneissic granites are strongly supported by the hydrous nature and mixed source characteristics (e.g., the presence of MMEs). The hydrous nature, as shown by the abundance of hydrous phases such as hornblende in the plutons, could be attributable to mixing of basaltic magma derived from a mantle- wedge previously metasomatized by subduction fluid/melt. Actually, the coeval metabasaltic rocks also show typical calc-alkaline affinity such as enrichment of LILEs (La, Th, Sr, Rb, etc.) and depletion of HSFEs (e.g., Nb, Ti) (Faure et al. 2004; Li and Chen 2014). Importantly, the gneissic granites show large variation in isotopic compositions with $\varepsilon_{Nd}(t) = -8.6$ to 1.5 and $\varepsilon_{Hf}(t) = -1.26$ to 5.59, which is consistent with the model of magma mixing between mantle-wedge derived basic magma and crustal melts in an arc setting.

As for the polarity of subduction, Bai (1993) proposed a northward subduction beneath the Longgang Block, while passive continental margin-type clastic sedimentary rocks were formed in the northern margin of the Rangnim Block. Final closure of the Paleoproterozoic ocean at ca. 1.9 Ga led to a continent-arc-continent collision and subsequent thrusting, forming the Liaoji Belt. In contrast, Faure et al. (2004) proposed a southward subduction beneath the Rangnim Block based on the fact that the South Liaohe Group is dominated by volcanic rocks. Our new zircon U-Pb data on the gneissic granites reveal the presence of some inherited zircons with ages of ~2500 and ~2700 Ma. These inherited zircons are in agreement with the age data reported for the TTG gneisses from the Longgang block that has received lots of U-Pb dating with ages ranging from 2500 to 3800 Ma but clustering at ~2500 and ~2700 Ma, which are commonly accepted as two major Archean crustal growth periods in the North China Craton (Zhao et al. 2001; Gao et al. 2004, 2005). By contrast, published data suggest that the Rangnim block contain rare rocks older than 2500 Ma (mainly 2440–2500 Ma; Wu et al. 2007a, b). So we can conclude that the source of the arc magmatism is mainly the lower crust beneath the Longgang Block in the north, which suggests a northward subduction in the Paleoproterozoic.

7.8 Conclusions

Most Paleoproterozoic gneissic granites in the Liaoji Belt are I-type granites, rather than A-type granites. The A-type features shown by some plutons (e.g., the Dafangshen pluton)

are attributable to extra addition of boron in the magma system, which have prolonged magma evolution, producing the highly evolved granites. The gneissic granites in the JLJB were formed at ca. 2.17–2.20 Ga, and were metamorphosed at ca. 1.9 Ga. These granites contain inherited zircons with Ahchean ages (ca. 2.5 Ga and 2.7–2.8 Ga). Based on the petrographical, mineralogical and geochemistry characteristics, we suggest that mixing/mingling of lower crust-derived felsic magma with enriched mantle-derived mafic magma might have resulted in formation of these gneissic granites. Overall, the petrology (common occurrence of hornblende, magnetite and sphene), geochemical data (the calc-alkaline affinity) and large variation of Nd–Hf isotopic data suggest that the Paleoproterozoic granites formed in a continental arc setting, rather than in a rifting setting as suggested by many other researchers.

References

Anderson, A. T. (1976). Magma mixing: Petrologicalprocess and volcanological tool. *Journal of Volcanologyand Geothermal Research, 1*, 3–33.

Bai, J. (1993). *The Precambrian geology and Pb–Zn mineralization in the northern margin of North China Platform*. Beijing: Geological Publishing House (in Chinese with English abstract).

Bai, J., & Dai, F.-Y. (1998). Archean crust of China. In X. Y. Ma, J. Bai (Eds.), *Precambrian crustal evolution of China* (pp. 15–86). Beijing: Springer Geological Publishing House (in Chinese with English abstract).

Bau, M. (1996). Controls on the fractionation of isovalent trace elements in magmatic and aqueous systems: Evidence from Y/Ho, Zr/Hf, and lanthanide tetrad effect. *Contribution to Mineralogy and Petrology, 123*, 323–333.

Bonin, B. (1990). From orogenic to anorogenic settings: Evolution of granitoid suites after a major orogenesis. *Geological Journal, 25*, 261–270.

Bonin, B. (2004). Do coeval mafic and felsic magmas in post-collisional to within-plate regimes necessarily imply two contrasting, mantle and crust, sources? A review. *Lithos, 78*, 1–24.

Cai, J.-H., Yan, G.-H., Mu, B.-L., Xu, B.-L., Shao, H.-X., & Xu, R.-H. (2002). U-Pb and Sm-Nd isotopic ages of an alkaline syenite complex body in Liangtun-Kuangdongguo, Gai County, Liaoning Province, China and their geological significance. *Acta Petrologica Sinica*, *18*, 349–354 (in Chinese with English abstract).

Chappell, B. W., White, A. J. R., Williams, I. S., Wyborn, D., & Wyborn, L. A. I. (2000). Lachlan Fold Belt granites revisited: High- and low-temperature granites andtheir implications. *Australian Journal of Earth Sciences, 47*, 123–138.

Chen, B., Chen, Z.-C., & Jahn, B.-M. (2009). Origin of mafic enclaves from the Taihang Mesozoic orogen, North China Craton. *Lithos*, *110*, 343–358.

Chen, B., Jahn, B.-M., & Suzuki, K. (2013). Petrological and Nd-Sr-Os isotopic constraints on the origin of high-Mg adakitic rocks from the North China Craton: Tectonic implications. *Geology, 41*, 91–94.

Chen, B., Ma, X.-H., & Wang, Z.-Q. (2014). Origin of the fluorine-rich highly differentiated granites from the Qianlishan composite plutons (South China) and implications for polymetallic mineralization. *Journal of Asian Earth Sciences, 93*, 301–314.

Chen, B., Tian, W., Jahn, B. M., & Chen, Z.-C. (2008). Zircon SHRIMP U-Pb ages and in-situ Hf isotopic analysis for the Mesozoic intrusions in South Taihang, North China Craton: Evidence for hybridization between mantle-derived magmas and crustal components. *Lithos, 102*, 118–137.

Chen, R.-D., Li, X.-D., & Zhang, F.-S. (2003). Several problems about the Paleoproterozoic geology of eastern Liaoning. *Geology of China*, *30*, 207–213 (in Chinese with English abstract).

Clynne, M. A. (1999). A complex magma mixing origin for rocks erupted in 1915, Lassen Peak, California. *Journal of Petrology, 40*, 105–132.

Faure, M., Lin, W., Monie, P., & Bruguier, O. (2004). Palaeoproterozoic arc magmatism and collision in Liaodong Peninsula (north-east China). *Terra Nova*, *16*, 75–80.

Feeley, T. C., Wilson, L. F., & Underwood, S. J. (2008). Distribution and compositions of magmatic inclusions in the Mount Helen dome, Lassen Volcanic Center, California: Insights into magma chamber processes. *Lithos, 106*, 173–189.

Gao, S., Rudnick, R. L., Yuan, H.-L., Liu, X.-M., Liu, Y.-S., Xu, W.-L., et al. (2004). Recycling lower continental crust in the North China Craton. *Nature*, *432*, 892–897.

Geng, Y.-S., Wan, Y.-S., & Shen, Q.-H. (2002). Precambrian basic volcanism and crustal growth in the North China Craton. *Acta Geologica Sinica*, *76*(2), 199–208.

Griffin, W. L., Wang, X., Jackson, S. E., Pearson, N. J., O'Reilly, S. Y., Xu, X., et al. (2002). Zircon chemistry and magma mixing, SE China: In-situ analysis of Hf isotopes. *Tonglu and Pingtan igneous complexes. Lithos, 61*, 237–269.

Guo, J.-H., Sun, M., Chen, F.-K., & Zhai, M.-G. (2005). Sm-Nd and SHRIMP U-Pb zircon geochronology of high-pressure granulites in the Sanggan area, North China craton: Timing of Paleoproterozoic continental collision. *Journal of Asian Earth Sciences*, *24*, 629–642.

Hao, D.-F., Li, S.-Z., Zhao, G.-C., Sun, M., Han, Z.-Z., & Zhao, G.-T. (2004). Origin and its constraint to tectonic evolution of Paleoproterozoic granitoids in the eastern Liaoning and Jilin province, North China. *Acta Petrologica Sinica*, *20*, 1409–1416 (in Chinese with English abstract).

He, G.-P., & Ye, H.-W. (1998a). Compositions and main characteristics of Early Proterozoic metamorphic terrains in the eastern Liaoning and the southern Jilin areas. *Journal of Changchun University Science and Technology*, *28*, 121–126 (in Chinese with English abstract).

He, G.-P., & Ye, H.-W. (1998b). Two types of Early Proterozoic metamorphism in the Eastern Liaoning and Southern Jilin provinces and their tectonic implications. *Acta Petrologica Sinica*, *14*, 152–162 (in Chinese with English abstract).

Holden, P., Halliday, A. N., & Stephens, W. E. (1987). Neodymium and strontium isotope content of microdiorite enclaves points to mantle input to granitoid production. *Nature, 330*, 53–56.

Huang, D.-Z., Gao, J., & Dai, T.-G. (2001). Geochemical tracing of the fluid in subduction zones. *Earth Science Frontiers*, *8*(3), 131–139 (in Chinese with English abstract).

Irber, W. (1999). The lanthanide tetrad effect and its correlation with K/Rb, Eu/Eu*, Sr/Eu, Y/Ho, and Zr/Hf of evolving peraluminous granite suites. *Geochimica et Cosmochimica Acta, 63*, 489–508.

Jahn, B.-M., & Ernst, W. G. (1990). Late Archean Sm-Nd Isochron Age for mafic-ultramafic supracrustal amphibolites from the Northeastern Sino-Korean Craton, China. *Precambrian Research, 46*, 295–306.

Jahn, B.-M., Wu, F.-Y., Capdevila, R., Martineau, F., Zhao, Z.-H., & Wang, Y.-X. (2001). Highly evolved juvenile granites with tetrad REE patterns: The Woduhe and Baerzhe granites from the Great Xing'an Mountains in NE China. *Lithos, 59*, 171–198.

Janoušek, V., Braithwaite, C. J. R., Bowes, D. R., & Gerdes, A. (2004). Magma-mixing in the genesis of Hercynian calc-alkaline granitoids:

An integrated petrographic and geochemical study of the Sázava intrusion, Central Bohemian Pluton, Czech Republic. *Lithos, 78*, 67–99.

Jiang, N., Guo, J.-H., & Chang, G.-H. (2013). Nature and evolution of the lower crust in the eastern North China Craton: A review. *Earth-Science Reviews, 122*, 1–9.

Kemp, A. I. S. (2004). Petrology of high-Mg, low-Ti igneous rocks of the Glenelg River Complex (SE Australia) and the nature of their interaction with crustal melts. *Lithos, 78*, 119–156.

Kemp, A. I. S., & Hawkesworth, C. J. (2006). Using hafnium and oxygen isotopes in zircons to unravel the record of crustal evolution. *Chemical Geology, 226*, 144–162.

Kröner, A., Compston, W., Zhang, G.-W., Guo, A.-L., & Todt, W. (1988). Age and tectonic setting of Late Archean greenstone–gneiss terrain in Henan Province, China, as revealed by single-grain zircon dating. *Geology, 16*, 211–215.

Leake, B. E., Woolley, A. R., Aprs, C. E. S., et al. (1997). Nomenclature of amphiboles: Report of the subcommittee on amphiboles of the international mineralogical association, commission on new minerals and mineral names. *The Canadian Mineralogist, 35*, 219–246.

Li, S.-Z., & Zhao, G.-C. (2007). SHRIMP U-Pb zircon geochronology of the Liaoji granitoids: Constraints on the evolution of the Paleoproterozoic Jiao-Liao-Ji belt in the Eastern Block of the North China Craton. *Precambrian Research, 158*, 1–16.

Li, S.-Z., Zhao, G.-C., Santosh, M., Liu, X., & Dai, L.-M. (2011). Palaeoproterozoic tectonothermal evolution and deep crustal processes in the Jiao-Liao-Ji Belt, North China Craton: A review. *Geological Journal*, *46*, 525–543.

Li, S.-Z., Zhao, G.-C., Sun, M., Han, Z.-Z., Hao, D.-F., Luo, Y., et al. (2005). Deformation history of the Paleoproterozoic Liaohe Group in the Eastern Block of the North China Craton. *Journal of Asian Earth Sciences*, *24*(5), 659–674.

Li, S.-Z., Zhao, G.-C., Sun, M., Hao, D.-F., Luo, Y., & Yang, Z.-Z. (2003). Paleoproterozoic tectonothermal evolution and deep crustal processes of the Jiao–Liao Block. *Acta Geologica Sinica*, *73*, 328–340 (in Chinese with English abstract).

Li, Z., & Chen, B. (2014). Geochronology and geochemistry of the Paleoproterozoic meta-basalts from the Jiao-Liao-Ji Belt, North China Craton: Implications for petrogenesis and tectonic setting. *Precambrian Research, 255*, 653–667.

Liu, D.-Y., Nutman, A. P., Compston, W., Wu, J.-S., & Shen, Q.-H. (1992). Remmants of ≥3800 Ma crust in the Chinese part of the Sino- Korean Craton. *Geology, 20*, 339–342.

Lu, X.-P., Wu, F.-Y., Guo, J.-H., Wilde, S. A., Yang, J.-H., Liu, X.-M., et al. (2006). Zircon U-Pb geochronological constraints on the Paleoproterozoic crustal evolution of the Eastern block in the North China Craton. *Precambrian Research*, *146*, 138–164.

Lu, X.-P., Wu, F.-Y., Guo, J.-H., & Yin, C.-J. (2005). Late Paleoproterozoic granitic magmatism and crustal evolution in the Tonghua region, northeast China. *Acta Petrologica Sinica*, *21*(3), 721–736 (in Chinese with English abstract).

Lu, X.-P., Wu, F.-Y., Lin, J.-Q., Sun, D.-Y., Zhang, Y.-B., & Guo, L.-C. (2004). Geochronological framework of early Precambrian granitic magmatism in the eastern Liaoning Peninsular: Constraints on the early Precambrian evolution of the Eastern Block of the North China Craton. *Chinese Journal of Geology*, *39*, 123–138.

Lu, L.-Z., Xu, X.-C., & Liu, F.-L. (1996). *Early Precambrian Khondalite Series in North China*. Changchun: Changchun Publishing House.

Lukkari, S., & Holtz, F. (2007). Phase relations of a F-enriched peraluminous granite: An experimental study of the Kymi topaz granite stock, southern Finland. *Contribution to Mineralogy and Petrology, 153*, 273–288.

Luo, Y., Sun, M., Zhao, G.-C., Ayers, J. C., Li, S.-Z., Xia, X.-P., et al. (2008). A comparison of U-Pb and Hf isotopic compositions of detrital zircons from the North and South Liaohe Group: Constraints on the evolution of the Jiao-Liao-Ji Belt, North China Craton. *Precambrian Research*, *163*, 279–306.

Luo, Y., Sun, M., Zhao, G.-C., Li, S.-Z., Xu, P., Ye, K., et al. (2004). LA-ICP-MS U-Pb zircon ages of the Liaohe Group in the Eastern Block of the North China Craton: Constraints on the evolution of the Jiao-Liao-Ji Belt. *Precambrian Research*, *134*, 349–371.

Ma, X.-H., Chen, B., & Yang, M.-C. (2013). Magma mixing origin for the Aolunhua porphyry related to Mo-Cu mineralization, eastern Central Asian Orogenic Belt. *Gondwana Research, 24*, 1152–1171.

Manning, D. A. C. (1981). The effect of fluorine on liquidus phase relationships in the system Qz-Ab-Or with excess water at 1 kb. *Contributions to Mineralogy and Petrology, 76*, 206–215.

Meng, E., Liu, F.-L., Cui, Y., & Cai, J. (2013). Zircon U-Pb and Lu-Hf isotopic and whole-rock geochemical constraints on the protolith and tectonic history of the Changhai metamorphic supracrustal sequence in the Jiao-Liao-Ji Belt, southeast Liaoning Province, Northeast China. *Precambrian Research, 233*, 297–315.

Noyes, H., Frey, F. A., & Wones, D. R. (1983). A tale of two plutons: Geochemical evidence bearing on the origin and differentiation of the Red Lake and Eagle Peak plutons, central Sierra Nevada, California. *Journal of Geology, 91*, 487–509.

Peccerillo, A., & Taylor, A. R. (1976). Geochemistry of Eocene calc-alkaline volcanicrocks from the Kastamonu area, Northern Turkey. *Contributions to Mineralogy and Petrology, 58*, 63–81.

Peng, Q.-M., & Palmer, M. R. (1995). The Palaeoproterozoic boron deposits in eastern Liaoning, China—A metamorphosed evaporite. *Precambrian Research, 72*, 185–197.

Peuct, J. J., Jahn, B.-M., & Cornichet, J. (1986). Zircon U-Pb age of a tonalite within the Qingyuan granite greenstone belt in Northeast China. In Chinese Academy of Geological Sciences (Ed.), *Contributions to international symposium of precambrian crustal evolution* (Vol. 3, pp. 222–229). Beijing: Geological Publishing House.

Sklyarov, E. V., & Fedorovsky, V. S. (2006). Magma mingling: Tectonic and geodynamic aspects. *Geotektonika*, *2*, 47–64.

Soderlund, U., Patchett, P. J., Vervoort, J. D. & Isachsen, C. E. (2004). The 176Lu decay constant determined by Lu-Hf and U-Pb isotope systematics of Precambrian mafic intrusions. *Earth and Planetary Science Letters, 219*(3-4), 311–324.

Sun, M., Armstrong, R. L., Lambert, R. S. J., Jiang, C.-C., & Wu, J.-H. (1993). Petrochemistry and Sr, Pb and Nd isotopic geochemistry of the Paleoproterozoic Kuandian Complex, the eastern Liaoning province, China. *Precambrian Research, 62*, 171–190.

Sun, S. S., & McDonough, W. F. (1989). Chemical and isotopic systematics of oceanicbasalts: Implications for mantle composition and processes. In: A. D. Sauders & M. J. Norry (Eds.), *Magmatism in the Ocean Basins* (Vol. 42, pp. 313–345). Geological Special Publications.

Tam, P. Y., Zhao, G.-C., Liu, F.-L., Zhou, X.-W., Sun, M., & Li, S.-Z. (2011). SHRIMP U-Pb zircon ages of high-pressure mafic and pelitic granulites and associated rocks in the Jiaobei massif: Constraints on the metamorphic ages of the Paleoproterozoic Jiao-Liao-Ji Belt in the North China Craton. *Gondwana Research*, *19*, 150–162.

Tam, P. Y., Zhao, G.-C., Sun, M., Li, S.-Z., Wu, M.-L., & Yin, C.-Q. (2012b). Petrology and meta-morphic P–T path of high-pressure mafic granulites from the Jiaobei massif inthe Jiao–Liao–Ji Belt, North China Craton. *Lithos*, *155*, 94–109.

Tam, P. Y., Zhao, G.-C., Zhou, X.-W., Sun, M., Guo, J.-H., Li, S.-Z., et al. (2012a). Metamorphic P-T path and implications of high-pressure politic granulites from the Jiaobei massif in the Jiao-Liao-Ji Belt, North China Craton. *Gondwana Research*, *22*, 104–117.

Vernon, R. H., Etheridge, M. E., & Wall, V. J. (1988). Shape and microstructure of microgranitoidenclaves: Indicators of magma mingling and flow. *Lithos, 22*, 1–11.

Wan, Y.-S., Song, B., Liu, D.-Y., Wilde, S.A., Wu, J. –S., Shi, Y.-R., et al. (2006). SHRIMP U-Pb zircon geochronology of Palaeoproterozoic metasedimentary rocks in the North China Craton: Evidence for a major Late Palaeoproterozoic tectonothermal event. *Precambrian Research*, *149*, 249–271.

Wang, H.-C., Lu, S.-N., Chu, H., Xiang, Z.-Q., Zhang, C.-J., & Liu, H. (2011). Zircon U-Pb age and tectonic setting of meta-basalts of Liaohe Group in Helan area Liaoyang, Liaoning Province. *Journal of Jilin University (Earth Science Edition)*, *41*, 1321–1334.

Wang, R.-M., Chen, Z.-Z., & Lai, X.-Y. (1997). Conversion from mantle plum regime to plate tectonic regime in North China. *Earth Sciences, 22*(3), 28–50.

Wang, W., Liu, S.-W., Wilde, S.A., Li, Q.-G., Zhang, J., Bai, X., et al. (2012). Petrogenesis and geochronology of Precambrian granitoid gneisses in Western Liaoning Province: Constraints on Neoarchean to early Paleoproterozoic crustal evolution of the North China Craton. *Precambrian Research*, *222–223*, 290–311.

Watson, E. B., & Harrison, T. M. (1983). Zircon saturation revisited: Temperature and composition effects in a variety of crustal magma types. *Earth and Planetary Science Letters, 64*(2), 295–304.

Whalen, J. B., Currie, K. L., & Chappell, B. W. (1987). A-type granites: Geochemical characteristics, discrimination and petrogenesis. *Contributions to Mineralogy and Petrology, 95*, 407–419.

White, A. J. R., Chappell, B. W., Wyborn, D. (1999). Application of the restite model to the Deddick granodiorite and its enclaves—A reinterpretation of the observations and data of Maas et al. (1997). *Journal of Petrology*, *40*, 413–421.

Wu, F.-Y., Han, R.-H., Yang, J.-H., Wilde, S. A., Zhai, M.-G., & Par, S. C. (2007a). Initial constraints on the timing of granitic magmatism in North Korea using U-Pb zircon geochronology. *Chemical Geology*, *238*, 232–248.

Wu, F.-Y., Yang, J.-H., Wilde, S. A., Liu, X.-M., Guo, J.-H., & Zhai, M.-G. (2007b). Detrital zircon U–Pb and Hf isotopic constraints on the crustal evolution of North Korea. *Precambrian Research*, *159*, 155–177.

Wu, Y.-B., & Zheng, Y.-F. (2004). Genetic mineralogy study on zircon and its restrict to explanation of U-Pb ages. *Chinese Science Bulletin*, *49*(16), 1589–1604 (in Chinese).

Yang, J.-H., Wu, F.-Y., Wild, S. A., & Zhao, G.-C. (2008). Petrogenesis and geodynamics of Late Archean magmatism in eastern Hebei, eastern North China Craton: Geochronological, geochemical and Nd-Hf isotopic evidence. *Precambrian Research*, *167*, 125–149.

Yin, A., & Nie, S. (1996). Phanerozoic palinspastic reconstruction of China and its neigh-boring regions. In A. Yin & T. M. Harrison (Eds.), *The tectonic evolution of Asia* (pp. 285–442). New York: Cambridge University Press.

Zhang, H.-F., Zhai, M.-G., Santosh, M., Diwu, C. R., & Li, S.-R. (2011). Geochronology and petrogenesis of Neoarchean potassic meta-granites from Huai'an Complex: Implications for the evolution of the North China Craton. *Gondwana Research*, *20*, 82–105.

Zhang, Q.-S. (1984). *Geology and metallogeny of the early Precambrian in China*. Jiling: Jilin People's Press.

Zhang, Q.-S., & Yang, Z.-S. (1988). *Early crust and mineral deposits of Liaodong Peninsula, China*. Beijing: Geological Publishing House (in Chinese with English abstract).

Zhao, G.-C., Sun, M., Wilde, S. A., & Li, S.-Z. (2005). Late Archean to Paleoproterozoic evolution of the North China Craton: Key issues revisited. *Precambrian Research, 136*(2), 177–202.

Zhao, G.-C., Wilde, S. A., Cawood, P. A., & Sun, M. (2001). Archean blocks and their boundaries in the North China Craton: Lithological, geochemical, structural and P–T constraints and tectonic evolution. *Precambrain Research, 107*, 45–73.

Zhao, G.-C., Wilde, S. A., Cawood, P. A., & Sun, M. (2002). SHRIMP U-Pb zircon ages of the Fuping Complex: Implications for accretion and assembly of the North ChinaCraton. *American Journal of Science, 302*, 191–226.

Zhou, X.-W., Zhao, G.-C., Wei, C.-J., Geng, Y.-S., & Sun, M. (2008). Metamorphic evolution and Th-U-Pb zircon and monazite geochronology of high-pressure pelitic granulites in the Jiaobei massif of the North China Craton. *American Journal of Science*, *308*, 328–350.